Morphology, stratigraphy, and mineralogical composition of a layered formation covering the plateaus around Valles Marineris, Mars: Implications for its geological history

L. Le Deit, Olivier Bourgeois, Laetitia Le Deit, E. Hauber, S. Le Mouelic, M. Massé, R. Jaumann, J.-P. Bibring

Morphology, stratigraphy, and mineralogical composition of a layered formation covering the plateaus around Valles Marineris, Mars: Implications for its geological history

L. Le Deit[1,2], O. Bourgeois[2], D. Mège[2], E. Hauber[1],

S. Le Mouélic[2], M. Massé[2], R. Jaumann[1], J.-P. Bibring[3]

[1]*Institute of Planetary Research, German Aerospace Center (DLR), Berlin, Germany.*

[2]*Laboratoire de Planétologie et de Géodynamique de Nantes, CNRS UMR-6112, Université de Nantes, France.*

[3]*Institut d'Astrophysique Spatiale, Université Paris 11, Orsay Campus, France.*

Submitted to Icarus October 14, 2009

Number of pages: 73

Number of figures: 19

Number of tables: 1

Proposed running head:

Layered formation above the Valles Marineris plateaus

Corresponding author:

Laetitia Le Deit

Email : Laetitia.Ledeit@dlr.de

Address : Institute of Planetary Research,

German Aerospace Center (DLR),

Rutherfordstr.2, 12489 Berlin, Germany

Phone: 0049-3067055338

Abstract

An extensive layered formation covers the high plateaus around Valles Marineris. Mapping based on HiRISE, CTX and HRSC images reveals these layered deposits (LDs) crop out north of Tithonium Chasma, south of Ius Chasma, around West Candor Chasma, and southwest of Juventae Chasma and Ganges Chasma. The estimated area covered by LDs is ~ 42300 km^2. They consist of a series of alternating light and dark beds, a hundred meters in total thickness that is covered by a dark unconsolidated mantle possibly resulting from their erosion. Their stratigraphic relationships with the plateaus and the Valles Marineris chasmata indicate that the LDs were deposited during the Early to Late Hesperian, and possibly later depending on the region, before the end of the backwasting of the walls near Juventae Chasma, and probably before Louros Valles sapping near Ius Chasma. Their large spatial coverage and their location mainly on highly elevated plateaus lead us to conclude that LDs correspond to airfall dust and/or volcanic ash. The surface of LDs is characterized by various morphological features, including lobate ejecta and pedestal craters, polygonal fractures, valleys and sinuous ridges, and a pitted surface, which are all consistent with liquid water and/or water ice filling the pores of LDs. LDs were episodically eroded by fluvial processes and were possibly modified by sublimation processes. Considering that LDs correspond to dust and/or ash possibly mixed with ice particles in the past, LDs may be compared to Dissected Mantle Terrains currently observed in mid- to high latitudes on Mars, which correspond to a mantle of mixed dust and ice that is partially or totally dissected by sublimation. The analysis of CRISM and OMEGA hyperspectral data indicates that the basal layer of LDs near Ganges Chasma exhibits spectra with absorption bands at ~1.4 µm, and ~1.9 µm and a large deep band between ~2.21 and ~2.26 µm that are consistent with previous spectral analysis in other regions of LDs. We interpret these spectral characteristics as an enrichment of LDs in opaline silica or by Al-phyllosilicate-rich layers being overlain by hydroxylated ferric

sulfate–rich layers. These alteration minerals are consistent with the aqueous alteration of LDs at low temperatures.

Keywords: GEOLOGICAL PROCESSES, MARS, SURFACE, MINERALOGY.

1. Introduction

Several studies have been performed on the internal layering of the plateaus surrounding the Valles Marineris canyon system on Mars (e. g. Treiman et al., 1995; Malin et al., 1998; McEwen et al., 1998; Malin and Edgett, 2000; Williams et al., 2003; Beyer and McEwen, 2005). The wall rocks of the Valles Marineris chasmata display layers that have been suggested to be flood basalts (McEwen et al., 1998) or lavas interbedded with sediments (Malin and Edgett, 2000), perhaps intruded by plutonic rocks (Williams et al., 2003). The ridged plain material that tops the plateau is interpreted as Hesperian lava flows (Scott and Carr, 1978).

An extensive light-toned layered formation covers the Hesperian and Noachian plateaus (Figure 1). In this paper, these layered deposits are designated as LDs. They correspond to the light-toned layered deposits (LLDs) described by Weitz et al. (2008, 2010), and by Bishop et al. (2009). The LD outcrops are exposed south of Ius Chasma (Milliken et al., 2007), southwest of Juventae Chasma (Lucchitta, 2005; Catling et al., 2006; Bishop et al., 2008; Williams and Weitz, 2010), and west of Ganges Chasma (Le Deit et al., 2008a-c, 2009 ; Weitz et al., 2008). Lucchitta (2005) noticed that several origins may explain the observed geological characteristics of LDs near Juventae Chasma. A material of volcanic origin such as ash is consistent with the light tone, the apparent fine grain size, the friability, the extent and the horizontal stratification of this formation (Lucchitta, 2005). The layering and flat lying “nature” of the LDs may also correspond to an eolian or glacial origin, similar to the Polar Layered Deposits. In that case, ice would have nucleated on eolian sands or dust deposited on the plateaus during past periods of high obliquity (Lucchitta, 2005). Sinuous ridges, interpreted as inverted channels are embedded in LDs near Juventae Chasma and Ganges Chasma (e.g., Williams et al., 2005; Weitz et al., 2008). From a morphologic analysis of the sinuous ridges and the LDs, Weitz et al. (2010) concluded that the strong correlation between both of these features argues for a fluvio-lacustrine environment.

Figure 1

From an analysis of data from the Compact Reconnaissance Imaging Spectrometer for Mars (CRISM), Swayze et al. (2007) found that the deposits south of Melas Chasma correspond to hydrated silicate glass. Milliken et al. (2008) demonstrated that H_2O- and SiOH-bearing phases most consistent with opaline silica and altered glass are detected in the LDs located south of Melas and Ius Chasma, between Melas Chasma and Juventae Chasma, and southwest of Juventae Chasma. Locally, they identified Fe sulfates, including jarosite, in association with the LDs. These characteristics are consistent with an extensive, low-temperature and acidic alteration of LDs during the late Hesperian and possibly the Amazonian (Milliken et al., 2008). On the plateau west of Juventae Chasma, opaline silica is found in thin layers superposed by hydroxylated ferric sulfates (Bishop et al., 2009; Murchie et al, 2009a). Recently, Roach et al. (2010) reported the occurrence of opal-rich deposits both on the plateau south of Ius Chasma, and a few kilometres below on the chasma floor at the outlet of the sapping valleys Louros Valles. Either these opal-rich deposits were transported into the chasma from the plateau by the sapping valleys, or the sediments were transported into the chasma and then altered to opal (Roach et al., 2010).

Despite these numerous studies, the source of sediment and water remains uncertain (Weitz et al., 2010). The analysis of the spatial extent and the morphological characteristics of LDs will help to constrain their emplacement mode, and hence their source. The study of the stratigraphy of LDs can also provide clues concerning their period of deposition in regard to the geological history of the region. The source of water may be investigated by the study of the link between the mineralogical composition of LDs and the associated morphological features.

The aim of our work is thus to constrain the spatial extent of the LDs, their stratigraphy, their morphology, their composition, their relative age, and to propose a model of emplacement that is consistent with all these characteristics. First, we report on the geomorphic mapping of the LDs, in particular in regions near Ius Chasma, Juventae Chasma and Ganges Chasma, where they are

clearly visible. We also explore their stratigraphical relationships with their environment. The following part presents the landforms associated with LDs and the corresponding constraints they provide to decipher the geological processes that occurred in the region. We report on the mineralogical composition of LDs near Ganges Chasma and in the other outcrop locations. Finally, we discuss our results, and conclude by suggesting a geological history for the LD setup.

2. Data and methods

2.1 Imaging and topographic data

From the analysis of visible and near infrared data, we have mapped the LDs cropping out on the plateaus in the region (Figure 2). Wherever available, we used data of the Context Camera (CTX) (~6 m/pixel) (Malin et al., 2007) and the High Resolution Imaging Science Experiment (HiRISE) (25-32 cm/pixel) (McEwen et al., 2007) instruments onboard the Mars Reconnaissance Orbiter. We also used the nadir panchromatic images of the High Resolution Stereoscopic Camera (HRSC) (12.5-30 m/pixel) (Neukum and Jaumann, 2004) and the color HRSC images, which provide almost a complete spatial coverage of the region of Valles Marineris. These data have been combined into a geographic information system using the Mars 2000 Sphere geographic coordinate system available in ArcGIS (equidistant cylindrical projection) (Seidelmann et al., 2002).

Topographic profiles across LDs are obtained with the gridded 128 pixel/° Mars Orbiter Laser Altimeter (MOLA) DEM and the MOLA PEDR single tracks (Smith et al., 2001). The minimum thickness of LDs is evaluated by calculating the elevation difference between the highest topographic points of LDs and the elevation of the stratigraphic contact between the basement and the LDs for each MOLA PEDR profile.

2.2 Hyperspectral imaging data

We used hyperspectral data in the visible near-infrared wavelengths to analyse the mineralogical composition of the LDs. In the targeted hyperspectral mode, the CRISM instrument provides 10 km x 10 km images with a high spatial resolution (18 m/pixel), and with a 544-channels spectrum between 0.362 µm and 3.92 µm for each pixel (Murchie et al., 2007, 2009b). The OMEGA imaging spectrometer onboard Mars Express provides a reflectance spectrum between 0.38 µm and 5.2 µm for each pixel of an image, the spatial resolution of which ranges between 300 m and 4.8 km/pixel (Bibring et al., 2004). The contribution of the atmosphere is removed from each OMEGA and CRISM spectrum using an empirical atmospheric transmission derived from the ratio between two spectra acquired at the top and the bottom of Olympus Mons, and scaled to the depth of the 2 µm CO_2 band (Langevin et al., 2005). For CRISM data analyses, this atmospheric correction is available in the CRISM Analysis Tool (CAT) (Murchie et al., 2007, 2009b) usable in the ENVI software. This set of routines also corrects data from the illumination angle, and georeferences images in the Mars 2000 coordinate system with an equirectangular projection.

For CRISM and OMEGA data, we focus on the 1.0 µm to 2.5 µm wavelength region, which is very diagnostic for identifying hydrated minerals commonly detected on Mars (i.e., phyllosilicates, sulfates, hydrated silica, and ferric oxides).

We calculated mean spectra of regions that were chosen for the characteristics of their spectral signatures. The selection of these regions of interest is often made by the study of spectral criteria maps (e.g., band ratios, band depths). We divided these mean spectra by spectra of neutral, homogeneous, and often dusty regions extracted from the same hyperspectral cube. This ratio method reduces the noise inherent to the data and emphasizes the absorption bands, reducing environmental effects such as dust and atmospheric residuals. It provides ratioed spectra, which can be directly compared to spectra of pure minerals acquired in laboratory.

3. Morphology, spatial distribution, and stratigraphy

3.1 Regional map

The LDs correspond to light-toned deposits cropping out on Sinai Planum, Lunae Planum, and Ophir Planum around the Valles Marineris chasmata (Figure 1). They differ from the basaltic basement by their higher albedo, their erosional style, their fine-grained appearance and the absence of any boulders at their surface. In many places, the rims of LD outcrops are parallel to the rims of the chasmata though they are located up to several hundreds of meters far from them (Figures 1c and 2). This suggests that LDs are weaker than the chasma wall material. They consist of subparallel finely layered deposits of various thicknesses draping the topography, and their total thickness does not exceed a hundred meters on average. The light-toned layers are apparently interbedded with darker beds (Figure 1b). This difference in albedo can be due to variations in mineralogical composition, topographic slope, roughness, grain size, state of erosion of the different layers or, to partial covering of certain layers by a dark mantle.

We have compiled a regional LD map around Valles Marineris (orange patches in Figure 2). In some cases their spatial extent is unclear due either to their being covered by a dark mantle (Figure 1b) or to the lack of high spatial resolution data. Dashed contours on Figure 2 outline these poorly constrained boundaries, whereas plain contours correspond to regions where the stratigraphic contact between the LDs and the underlying basement is unambiguous. We have identified and mapped LDs north of Tithonium Chasma, south of Ius Chasma, around West Candor Chasma, and southwest of Juventae Chasma and Ganges Chasma. The estimated minimal area currently covered by LDs is ~ 42300 km^2, which corresponds to ~1/5 of the surface area of layered deposits in Meridiani Planum (2 x 10^5 km^2) (Hynek et al., 2004). The largest LD outcrops are located south of Ius Chasma; they occupy ~ 29500 km^2 and represent ~ 70 % of the total mapped surface. The LDs near Juventae Chasma and Ganges Chasma cover ~2300 km^2 and ~300

Figure 2

km^2 respectively. These estimated values correspond to minimal present-day values because of the unclear boundaries. In the past, LDs certainly covered much larger areas since many erosional remnants buttes of LDs are located up to several tens of kilometres from the main outcrops (Figures 6 and 8). At least ~ 2300 km^2 of LDs were removed from the plateaus near Juventae Chasma if we make the hypothesis that LDs were previously located between the main outcrops, the remnant buttes, and the pedestal craters (gray surface in Figure 6b). Hence, this rough approximation suggests that at least half of the LDs originally deposited in the region would have been removed so far. Taking into account that the current total thickness of LDs in this region is ~50 m, the volume of material removed would correspond to more than 100 km^3.

LDs are mainly located on top of plateaus along chasmata walls (Figure 2). Outcrops of LDs are also located in depressions such as a hanging depression south of Melas Chasma (Quantin et al., 2005) (Figures 2, 3, and 5), and in pits southwest of Juventae Chasma (Weitz et al., 2010) (Figure 6). Even if these deposits are located inside chasmata or pits, they display similar layering and morphologies as the deposits located on the plateaus. We therefore interpret them as LDs rather than as Interior Layered Deposits (ILDs) (e.g., Lucchitta et al., 1992), which are commonly thick (several 1000 m) and fluted (e.g., Nedell et al., 1987).

3.1.1 LDs south of Ius Chasma

Morphostratigraphic relationships between LDs, basement, chasmata, and fluvial features provide constraints on the relative age of emplacement and erosion of LDs. South of Ius Chasma, LDs overlay Noachian, Early and Late Hesperian terrains corresponding to ridged plains material (units Nplr, Hr, and Hsu on the geological map of Witbeck et al. (1991)) (Figure 3). These terrains are interpreted as lava flows erupted from local fractures (and from the summit of Syria Planum for the Hsu unit) (Witbeck et al., 1991). The LD unit is stratigraphically above the

Figure 3

Hesperian units Hr and Hsu, which are themselves stratigraphically above the Noachian unit Nplr. LDs are consequently younger than the youngest Hesperian unit Hsu. Thus, the maximum age of emplacement of LDs on the plateau south of Ius Chasma is Late Hesperian. Some valleys incised in the LDs are connected to the heads of Louros Valles (Figure 4), which probably result from sapping processes (Kochel and Piper, 1986; Lucchitta et al., 1992). Sapping is thought to correspond to the backward incision of canyons due to circulation and seepage of groundwater (e.g., Laity and Malin, 1985). Mangold et al. (2008) studied shallow valleys carved in a thin and weak unit (different from LDs) overlying the plateaus around Echus Chasma. Many outlets of these shallow valleys are connected to the head of Echus Chasma canyons that have most probably been produced by sapping processes (Mangold et al., 2008). These canyons may have formed coevally with these shallow valleys (Mangold et al., 2008). Valleys incised in the LDs connected to the head of Louros Valles may have similarly contributed to sapping, these valleys and Louros Valles being coeval. It would imply that the LDs were deposited before the formation of Louros Valles. Roach et al. (2010) detected some opal-rich deposits in Ius Chasma at the outlet of Louros Valles that were transported into the chasma from the plateaus by the sapping valleys. This suggests that the LDs were deposited on the plateaus before the formation of Louros Valles.

In the depression to the east adjacent to Melas Chasma, LDs mantle a faulted basement outcrop (Figure 5a-b), which probably tilted during the opening of the hanging depression. LDs are also observed in the hanging depression. Quantin et al. (2005) identified layered deposits on the walls and in the bottom of the hanging depression. Due to their alternating bright and dark layering, and to the absence of any ventifacts such as flutes or yardangs on their surface, we associate these layered deposits to LDs rather than to ILDs. Quantin et al. (2005) identified valley networks carved in these LDs (Figure 5a,d). At the outlet of these valleys, delta deposits and subhorizontal layers in an enclosed depression probably correspond to lacustrine deposits (Quantin et al., 2005;

Figure 5

Metz et al., 2009) (Figure 5a). All the features observed in this hanging depression are dated from the Late Hesperian (Quantin et al., 2005).

Stratigraphic relationships suggest the following succession of events happened south of Ius Chasma: (1) Emplacement of Sinai Planum lavas from Noachian to Late Hesperian; (2) Tectonic opening of the hanging depression; (3) Emplacement of LDs on the plateaus and in the hanging depression; (5) Fluvial erosion of LDs in the hanging depression and on the plateaus; (6) Deposition of the erosion products of LDs in deltas and in a lake during the Late Hesperian; Backward incision of Louros Valles. Roach et al. (2010) showed that the erosion products of the LDs were then transported at the outlet of Louros Valles.

3.1.2 LDs southwest of Juventae Chasma

Southwest of Juventae Chasma, LD outcrops are located stratigraphically above ridged plains material, which is dated from the Early Hesperian (unit Hr in Witbeck et al., 1991) (Figure 6 a-b). In this region, LDs are consequently Early Hesperian in age or younger. The Hr unit displays wrinkle ridges striking West-East (Lucchitta, 2005) (Figure 6). LDs lie subhorizontally on the plateau and they have not been folded or faulted by the formation of the wrinkle ridge. As a consequence, LD deposition postdates the formation of the wrinkle ridges. The study of the erosive rim of LDs along the chasma wall provides insights about the chronological relationships between the deposition of LDs and the backwasting of Juventae Chasma walls. A tilted basement block is located along the southern wall of the chasma (Figure 7). A thin sequence of LDs covers the summit of the tilted block. The tilt of this sequence, and the occurrence of sinuous ridges, which are not striking parallel to the direction of the current steepest slope indicate that LDs were deposited there before the tilting of the block. Hence, LDs were deposited before the end of the backwasting of Juventae Chasma walls.

Figure 6

Figure 7

3.1.3 LDs southwest of Ganges Chasma

Southwest of Ganges Chasma, LDs are located stratigraphically above Noachian terrains that are defined as a subdued cratered unit (unit Npl2 in the map of Scott and Tanaka (1986) and Witbeck et al. (1991)) (Figure 8). This unit has been interpreted as thin interbedded lava flows and eolian deposits that partly bury underlying rocks (Scott and Tanaka, 1986). The Noachian unit Npl2 is incised by the outflow channel Allegheny Vallis running between the Ophir Cavus pit and Ganges Chasma. The flow that has carved Allegheny Vallis and isolated islands ("scablands") in the Npl2 unit (Figure 8) occurred during the mid- to late-Hesperian (Coleman et al., 2007). LDs are located stratigraphically above Allhegheny Vallis, so they are mid to late-Hesperian in age or younger.

Figure 8

From stratigraphic relationships, we can conclude that LDs were deposited during the Early to Late Hesperian, and possibly later depending on the region, before the end of the backward wall erosion near Juventae Chasma, and probably before the formation of Louros Valles by sapping processes near Ius Chasma.

3.1.4 Dark mantle

A dark mantle covers most LD outcrops (Figure 1b-c). THEMIS IR nighttime mosaics show that the brightness temperature of the LD surface is lower than that of the surrounding terrains (Figures 3c, 6c, 8c). In order to evaluate the thermal inertia of the LD surface, we have calculated the average TES thermal inertia (Putzig et al., 2007) of LDs in each region as a function of their area (Figure 9). As an example, LDs near Juventae Chasma correspond to 5.5 % of the LDs, and the thermal inertia of their surface reaches 315 SI. Around 90 % of the LD surface mapped so far is characterized by a thermal inertia value $\leq$ 200 SI, which is usually interpreted as fine-grained and/or unconsolidated material (Mellon et al., 2000). We do not associate this material to the LDs

Figure 9

themselves but to the dark surficial mantle that covers most outcrops of LDs. Indeed, the small and fresh outcrops of LDs (indicated by arrows in Figure 3c) display a higher brightness temperature than both the LD surface and the surrounding terrains. The thermal inertia of the LD surface in the hanging depression of Melas Chasma, near Juventae Chasma and Ganges Chasma is generally higher (> 300 SI) than in the other regions (Figure 9). This may be due to the dark mantle being indurated.

The location of the low brightness temperature dark mantle exactly matches the location of LDs (Figures 3, 6, and 8). As a consequence, the dark mantle could correspond to an erosion product of the LDs accumulated as lag deposits on the surface of the LDs. In this case, the dark beds in the LDs would correspond to beds enriched in this dark material, which would be more resistant to erosion than the light material. However, the possibility that the surface of the LDs favours the accumulation of eolian fines relative to the surfaces of the adjacent lava plains cannot be ruled out.

3.2 Associated landforms

The surface of LDs is characterized by various landforms: lobate ejecta and pedestal craters, polygonal fractures, valleys and sinuous ridges, and sublimation features. These landforms provide insights about the role that liquid and solid water played in the geological history of the LDs. Hereafter, we describe these landforms and discuss their implications.

3.2.1 Lobate ejecta and pedestal craters

Like most Martian surfaces, LDs are dotted with impact craters. Peulvast et al. (2001) reported lobate ejecta blankets of impact craters on plateaus around Valles Marineris. Some impact craters on LDs near Tithonium, Candor, Ius, Juventae, and Ganges chasmata are characterized by lobate

Figure 10

ejecta (Figure 10). Locally, ejecta lobes terminate distally in ramparts (Figure 10a). This kind of ejecta corresponds to fluidized deposits induced by the presence of volatile elements (liquid water or water ice) in the ground during the impact (e.g. Carr et al., 1977; Mouginis-Mark, 1979; Peulvast et al., 2001) and/or by winds generated in the atmosphere by the impact (e.g., Schultz and Gault, 1979; Barnouin-Jha et al., 1996, 1999a and b). Even if the relative role of these two processes is not well constrained, the role of the subsurface water is largely favoured (e.g., Baratoux et al., 2005). In this hypothesis, the impact releases a high amount of energy in the form of heat, which induces fusion and/or sublimation of volatile elements contained in the ground. Ejecta that are thus enriched in volatiles flow like debris flows or mud flows and form the observed lobes (e.g. Carr et al., 1977).

Other ejecta morphologies are also identified on LDs. They correspond to pedestal craters, which are observed on LDs near Juventae Chasma (Lucchitta, 2005; Figure 6b) and Ganges Chasma (Figure 10c-d). They are characterized as outward-facing scarps bordering a plateau perched tens of meters above the surrounding terrains (McCauley et al., 1973). LDs crop out under the ejecta blanket of these pedestal craters (Figure 10c-d). One hypothesis for their formation is that a fine-grained substrate (the LDs) was armoured during the impact event and was protected from subsequent eolian deflation that removed the surrounding LDs (e.g., Arvidson et al., 1976). Some authors propose that pedestal craters may have formed like craters with lobate ejecta; the volatile elements in the substrate during the impact would imply the fluidization of ejecta and then their armouring (e.g., Mouginis-Mark, 1979). Recent studies show that most pedestal craters are located at latitudes poleward of ~40° (e.g., Barlow, 2005; Kadish et al., 2008, 2009). Some pedestal craters are also observed in near-equatorial regions such as on the Medusae Fossae Formation (Kadish et al., 2008). Authors propose that the substrate surrounding the armoured region corresponded to ice-rich material deposited during periods of high obliquity (e.g., Kadish

and Barlow, 2006). During low obliquity periods, the ice-rich substrate is preferentially removed by sublimation of ice, leaving the ejecta blankets perched above the surroundings.

Lobate ejecta and pedestal craters are both consistent with a substrate enriched in volatile elements. These landforms suggest that LDs were enriched in volatile elements such as liquid water and/or water ice during the impact events. LDs surrounding the pedestal craters may have been removed by eolian deflation and/or sublimation during periods of low obliquity.

3.2.2 Polygonal fractures

Many layers of LDs display polygonal fractures on their surfaces (Figure 11) (Le Deit et al., 2008a-c; Weitz et al., 2010). The dark mantle locally fills the fractures between the polygons, which are characterized by different shapes and sizes. On Earth, polygons can be associated with different types of environments, climates and formation processes. In periglacial regions, they often indicate the occurrence of ground ice and temperature variations (e.g., Rapp and Clark, 1971). On Mars, many polygons occur in high latitude regions (above 55° in latitude) and are interpreted as effects of seasonal temperature variations such as thermal contraction and seasonal thaw (e.g., Mangold et al., 2005).

Figure 11

Some polygons observed on LDs have irregular shapes and are meter-scale in size (Figure 11a). This kind of polygon is quite common on the Martian sedimentary rocks and does not require the presence of water to form (Mangold et al., 2005). Other polygons have more regular shapes, they are flat-topped, and reach a few dozens of meters in size (Figure 11b). According to the classification of polygonal networks made by Mangold et al. (2005), they correspond to a random orthogonal network that implies a homogeneous formation process. These random orthogonal networks of cracks in the LDs may result from thermal contraction due to an ancient ice-rich substrate, to desiccation, or to partial dehydration of minerals. Similar random orthogonal

networks have been observed in phyllosilicate-rich layers in Mawrth Vallis (e.g., Loizeau et al., 2007), and on outcrops enriched in Mg-rich sulfates of Meridiani Planum (e.g., Squyres et al., 2006), and could therefore result from the same formation process.

3.2.3 Valleys and sinuous ridges

Description and interpretation of valleys

Valleys are carved in LDs near Ius, Melas, Candor, Juventae, and Ganges Chasmata (e.g., Williams et al., 2005; Weitz et al., 2008, 2010; Le Deit et al., 2009; Williams and Weitz, 2009). Near Juventae Chasma, some subparallel valleys form a low order network (Figure 12a, Williams and Weitz, 2009). They are characterised by a V-shape cross-section that is diagnostic of fluvial channels. These channels form a network, which is similar to immature terrestrial drainage networks that suggest the fluvial system was short-lived (Williams and Weitz, 2009).

Figure 12

West of this fluvial system, sinuous valleys incised in the Hesperian basement are visible on HiRISE images (Figure 12b) (Le Deit et al., 2009; Weitz et al., 2010). Their direction is parallel to the direction of the steepest slope. Locally, sinuous ridges fill these valleys indicating that the valleys are stratigraphically below the LDs, and hence that they are older than LDs.

In the hanging depression southwest of Melas Chasma, valleys form high order valley networks (Figure 5d) (Quantin et al., 2005). The valleys are 50 m to 2 km wide, and a few meters to 150 m deep. Their drainage density is of the same order of magnitude as that of terrestrial hydrographic networks studied at the same resolution (i.e., 1.5 km^{-1}, Quantin et al., 2005). The dense, hierarchized, and mature networks suggest that these valley networks result from runoff of precipitation, and that the system probably lasted at least several thousands years (Quantin et al., 2005).

All these valleys indicate that fluvial erosion occurred in LD regions before and after LD emplacement. The maturity variations between the different systems indicate that the fluvial activity was short-lived to long-lived depending on the region and possibly on the epoch.

Description of sinuous ridges

Sinuous ridges are observed in LDs near Juventae Chasma (Figure 13; e.g., Lucchitta, 2005; Mangold et al., 2008; Williams and Weitz, 2009), Ganges Chasma (Figure 8b; Williams et al., 2005; Le Deit et al., 2008b, 2009), and possibly Ius Chasma (Weitz et al., 2010). The brightness temperature of the material constituting these sinuous ridges is also similar to that of LDs (Figures 6c, and 8c); this suggests they are composed of the same material. Some LDs are capped by sinuous ridges (Figure 13c). The latter probably protect these LDs from erosion (Lucchitta, 2005). The sinuous ridges are linear or curvilinear; some of them are interconnected and form in some cases branched to dendritic networks. This type of network suggests that ridges correspond to ancient channels in which a fluid flowed. Some ridges near Juventae Chasma form a dendritic system of ~1500 km^2 (Figure 13a). The ridges strike North-Northeast and follow the regional slope of 0.2° N (Mangold et al., 2008). Upstream ridges are located at the foot of wrinkle ridges striking West-East (Figure 13a). Many ridges are not disrupted and can reach up to ~12 km in length. Ridges are up to a dozen meters wide in the southern part and they widen towards the northern part, where they can reach 300 m in width. This suggests flowing toward the North (Mangold et al., 2008). Some ridges display singular morphologies suggesting they are inverted cut-off meanders (Figure 13b). This kind of feature is characteristic of fluvial morphologies.

Figure 13

In the northern part of the LDs near Juventae Chasma, some ridges are more linear and roughly parallel to each other (Figure 13d). They constitute branched networks that strike NW-SE and

NE-SW. Both of them are located along the border of the main LD outcrop and follow the regional topographic slope.

Sinuous ridges near Ganges Chasma are simple or branched and are characterized by a mean length of 500 m (Figure 8b). They are consequently shorter than the ones near Juventae Chasma. The local slope is ~0.6° toward the southwest, and the ridges converge in this direction; this suggests a flow from Northeast to Southwest. One of these ridges is very well preserved and is only partially exhumed. Almost continuous, it measures ~17 km in length and between ~40 m and ~150 m in width, and it crosses the LDs from West to East. North and south of this ridge, the erosion surface of LDs display parallel valleys striking normal to the ridge. They may result from eolian erosion or runoff at the surface of LDs. Weitz et al. (2010) propose that from a planimetric view this ridge and valleys could correspond to a deltaic system, the hills between the valleys corresponding to non exhumed ridges.

Sinuous ridges are located at different stratigraphic levels in LDs. Some are almost in contact with the basement (e.g., Figure 12), others are located several dozens of meters above the base of LDs, and some appear at the summit of the LD series (e.g., Figure 13c). It suggests that sinuous ridges formed at different times during LD deposition.

Interpretation of sinuous ridges

Different hypothesis have been proposed to explain the morphology of sinuous ridges in these regions. Their positive relief is consistent with eskers, which correspond to material deposited by subglacial flows (e.g., Banerjee and McDonald, 1975). Eskers can be branched upstream and downstream, and they form anastomosing networks in which ridges superpose each other (e.g., Evans, 2005). This is not observed in our study area. Furthermore, the presence of a dendritic and

hierarchized network near Juventae Chasma suggests another emplacement process prevailed for these ridges.

Our favoured hypothesis is that sinuous ridges correspond to inverted fluvial channels (e.g. Mangold et al., 2005; Williams et al., 2005; Weitz et al., 2008, 2010; Williams and Weitz, 2009). Inverted features result from the differential erosion of the material deposited in the channels, which is more competent than the surrounding materials. Either the material deposited in the channels is more competent due its lithology, or fluid circulations increased its induration. The presence of sulfates in the material may have also contributed to its cementation, making it more resistant to erosion than the surrounding materials. Considering the hypothesis that sinuous ridges are inverted channels, they correspond to airfall material or to the erosion product of LDs that have been deposited in liquid water-filled valleys. Such an emplacement mode for sinuous ridges is reinforced by the occurrence of the valleys in almost all regions of LDs.

If LDs corresponded to a mixture of ice and dust/ash particles, warming of the LDs by an episodic climate change due to a change in obliquity, a punctual event (such as an impact event (e.g. Segura et al., 2002), or a seismic event) or a geothermal anomaly (e.g., associated to Tharsis volcanic activity, Phillips et al., 2001) may have resulted in partial melting of the ice contained in the LDs, its percolation though the pores of the LDs and then its concentration in channels of water charged of dust/ash particles following the regional slope. Another possibility is that the ridges and valleys result from runoff of precipitation (rain or molten snow) on the LDs (Mangold et al., 2008).

Valleys and sinuous ridges attest that fluvial erosion and deposition occurred on the plateaus around Valles Marineris before, during, and after the emplacement of the LDs. Liquid water required for the fluvial erosion originated from precipitation and/or melting of the ice contained in the LDs.

3.2.4 Pitted texture

The current surface of the LDs near Juventae Chasma displays a pitted texture (Figure 14b). The smallest pits are circular to ovoid depressions, 10 m in diameter, and larger ones are disrupted shaped-depressions, hundreds of meters in width. The smallest pits are easily distinguishable from simple impact craters since the depressions have no raised rims.

Figure 14

Williams and Weitz (2009) interpret these pits as heterogeneities in LDs. We suggest an alternative interpretation, based on the comparison of the pitted texture of LDs to scalloped pits occurring in the Dissected Mantle Terrain (DMT) in Tempe Terra, located ~50° north to LDs (Figure 14a). The DMT corresponds to meters-thick layers of dust mixed with ice, in which sublimation of interstitial ice resulted in the formation of scalloped pits (e.g., Mustard et al., 2001; Milliken et al., 2003; Morgenstern et al., 2007; Lefort et al., 2009). They can coalesce and form larger pits similar to those we observe on LDs. Therefore we infer that the pits observed in the LDs correspond to small collapse structures resulting from sublimation of ice contained in the LDs.

Morphological features associated with LDs testify that water played a role in their geological history. The presence of liquid water and/or water ice in LDs during impact events resulted in craters with lobate ejecta. The water ice in the LDs may be responsible for their polygonal fracturation. Liquid water originating from precipitation and/or melting of ground ice episodically eroded the LDs by fluvial processes during and after their emplacement. Eventually, the surface of the LDs displays a pitted texture, which is most probably due to sublimation processes.

4. Mineralogical composition

4.1 Spectral properties of LDs southwest of Ganges Chasma

Detailed analyses of LDs near Ius Chasma, Melas Chasma, Candor Chasma, Juventae Chasma and Ganges Chasma, based on CRISM data, have been published recently (Milliken et al., 2008; Bishop et al., 2009; Weitz et al., 2010). We analysed LDs near Ganges Chasma with both CRISM and OMEGA data since no minerals have been detected over most of these LDs so far (Le Deit et al., 2009). In addition, the integration of both CRISM and OMEGA data sets provides a better confidence level in the detection when spectral features can be seen by the two independent instruments. The careful analysis of hyperspectral data shows no characteristic spectral signature associated with the LD topographic surface. HiRISE and CTX data show that this surface is mostly covered by the dark material mantling the LDs there as in other regions (see part 3.1.4). TES analyses indicate that the thermal inertia of this material is ~403 SI, which corresponds to material competent enough to have spectral absorption bands (Figure 9). Consequently, the dark material corresponds to a spectrally neutral material.

The CRISM cube FRT 8949 covers the topographic surface of LDs, and their border along the Ganges Chasma wall (Figure 15). Some spectra exhibit small absorption bands at ~1.4 µm, ~1.9 µm and a deep and wide band between ~2.21 and ~2.26 µm (Figure 16a-c), in agreement with Weitz et al. (2010). These spectral characteristics are diagnostic of hydrated minerals. One OMEGA pixel (orbit 0394_2) located on LDs shows similar spectral properties, which reinforces the confidence in the detection (Figure 16c). The comparison of CRISM data with HiRISE image PSP_005939_1720 shows that the hydrated minerals correspond to a small bright outcrop located at the stratigraphic contact between the basement and the series of LDs (Figure 16a-b). All bright outcrops located at the same stratigraphic level display similar spectral properties (arrows on Figure 16a). This basal layer, which is hence characterised by the same mineralogical

Figure 15

Figure 16

composition, is bright and displays polygonal fractures that are often filled in with dark material (Figure 16d).

4.2 Comparison with spectral properties of other LDs and interpretations

Figure 17

Spectra associated with some LDs display a weak to strong absorption band at 1.9 μm, which is typical of hydrated minerals. Near Ius Chasma, Melas Chasma, and Juventae Chasma and in the hanging depression south Melas Chasma, they exhibit an additional band at ~1.41 μm, and a wide band with a minimum at ~2.21 μm (Milliken et al., 2008; Weitz et al., 2010) (Figure 17). Band positions and global shapes of ratio spectra for these layers of LDs are similar to those near Ganges Chasma, which suggests that they constitute the same compositional unit. Several minerals are consistent with the observed spectral characteristics. The band centered at ~2.21 μm may be due to Al-OH bonds and/or Si-OH bonds (Milliken et al., 2008). Si-rich phases such as opaline silica and chalcedony are good candidates to explain the large width and the asymmetry of the band between ~2.21 μm and ~2.26 μm (Anderson and Wickersheim, 1964) (Figure 17). The band at ~2.2 μm is generally narrower and symmetric for Al-rich phyllosilicates such as montmorillonite and palygorskite (Figure 17). Milliken et al. (2008) noticed that the asymmetry at the long wavelength edge of this band and the OH absorption at ~1.38 μm rather than ~1.41 μm can be criteria to distinct opaline silica from Al-OH phyllosilicates or hydrated glass. However, linear mixing of a spectrum of montmorillonite with a spectrum of an iron-rich sulfate with Fe-OH bonds (e.g. jarosite) produces a spectrum with an asymmetric band at ~1.4 μm (Figure 17). This synthetic spectrum fits the band observed on CRISM spectra of the LDs. Consequently, opaline silica or a linear mixture of Al-rich phyllosilicates and a mineral that has Fe-OH bonds (e.g. hydroxylated ferric sulfate) may explain the observed spectra. The detection of jarosite by Milliken et al. (2008) and Weitz et al. (2010) near Melas Chasma reinforces the

possibility of the occurrence of this kind of mixture in LDs. Indeed some layers also exhibit spectra with absorptions at ~1.85 µm and ~2.26 µm, which is diagnostic of jarosite absorption bands (Figure 17).

LDs near Juventae Chasma display two distinct phases: an opaline silica phase (characterized by a broad absorption band at ~2.21 µm) and a hydroxylated ferric sulfate (characterized by a narrow Fe-OH combination band at 2.23 µm) (Bishop et al., 2009). The opaline silica phase is associated with a layer located at the contact between the cratered plateau and the series of LDs (Figure 18). The layer appears "cracked and fragmented" (Weitz et al., 2010), and has a "broken and blocky texture" (Bishop et al., 2009). This layer at the base of LDs near Juventae Chasma has consequently similar morphological characteristics and mineralogical composition as the basal layer of LDs near Ganges Chasma (Figure 18). The outcrops of the basal layer of LDs near Juventae Chasma appear however fresher than those near Ganges Chasma. The second mineralogical phase detected in LDs near Juventae Chasma is located stratigraphically above the basal layer, and is enriched in hydroxylated ferric sulfate (Bishop et al., 2009). It is spectrally characterized by absorption bands at ~1.4 µm (OH overtone), ~1.94 µm (H_2O band), ~2.23 µm (metal-OH band) and a shoulder near 2.4 µm (Figure 17). According to Bishop et al. (2009), it could correspond to partially dehydrated ferricopiapite (Milliken et al., 2008; Weitz et al., 2010), H_3O^+-jarosite (Desborough et al., 2006), or szomolnokite (Morris et al., 2009). These layers enriched in hydroxylated ferric sulfate consist of alternating bright and dark layers like most LDs. Considering that LDs near Juventae Chasma and Ganges Chasma have many similar morphological and mineralogical characteristics (i.e., a basal layer – whose corresponding spectra are characterized by a broad absorption band at ~2.21 µm-, a series of bright and dark layers, and many sinuous ridges), these LD have probably registered a common and contemporaneous geological history.

Figure 18

4.3 Implications

Hydrated minerals are detected in LDs. In most of cases, the corresponding layers contain opaline silica or a mixture of Al-rich phyllosilicates and hydroxylated ferric sulfates. Near Juventae Chasma and Ganges Chasma, this mineralogical composition is present in the basal layer of LDs, in contact with the basement. Stratigraphically above this basal layer, layers are enriched in hydroxylated ferric sulfates near Juventae Chasma. The stratigraphic contact between these layers and the basal layer reinforces the hypothesis that the basal layer may correspond to a mixture of Al-rich phyllosilicates and hydroxylated ferric sulfates. Near Melas Chasma, this material is at the same stratigraphic level as jarosite (Weitz et al., 2010), which is clearly identified in that case by the presence of an absorption band at ~1.85 µm. Milliken et al. (2008) suggests that the detected jarosite corresponds to non-stoichiometric, Fe-deficient, H_3O-bearing jarosite. Indeed, this type of jarosite can form by precipitation under low-temperature acidic conditions, and does not require high temperatures such as hydrothermal processes to form (Stoffregen et al., 2000; Milliken et al., 2008; Weitz et al., 2010). The basal layer in LDs near Juventae Chasma and Ganges Chasma may be enriched in opaline silica. The stack of layers resting stratigraphically above it is enriched in hydroxylated ferric sulfates in the Juventae Chasma region. This sequence is consistent with the evaporation of fluids produced by the acidic dissolution of basaltic material with low water-to-rock ratios (Tosca et al., 2004; Hurowitz et al., 2005; Milliken et al., 2008). Another possibility is that the basal layer is enriched in Al-rich phyllosilicates, and that remnants of the upper unit enriched in Fe sulfates lay on its surface. In that case, this contact would record a change in the geochemical conditions by the transition between neutral aqueous alteration and acidic aqueous alteration. In all cases, the mineralogical species identified in LDs are consistent with alteration products of basaltic material at low temperatures. It is in agreement with the

morphological study of LDs that shows that water was present in LDs during its geological history, and was originating from precipitation.

5. Discussion

5.1 Comparison between the LDs

The geological analysis of LDs showed that they display both similarities and disparities between the different regions (Figure 19). The LDs near Juventae Chasma and Ganges Chasma share many common properties. They are characterized by a comparable total thickness (less than 50 m), the occurrence of remnant buttes, pedestal craters, sinuous ridges and valleys, and a similar stratigraphic organization based on a basal bright and deeply fractured unit of similar spectral characteristics overlain by a series of light and dark layers (Figure 19a-b). However, the mineralogical composition of this latest unit could not be constrained near Ganges Chasma. These similar properties suggest that LDs near Juventae Chasma and Ganges Chasma record similar geological events, which may have occurred coevally. Similarly, the LDs near Ius Chasma and in the hanging depression near Melas Chasma share many common properties and are located geographically close to each other (Figure 19c-d). Thick series of LDs are preserved in these regions, which do not display sinuous ridges (except for possible sinuous ridges located near Ius Chasma and identified by Weitz et al., 2010). LDs are carved by many valleys in these locations. Moreover, fluvial erosion of LDs resulted in the formation of lacustrine deposits in the hanging depression. LDs located on the plateaus near Ius Chasma and in the hanging depression near Melas Chasma are both characterized by the presence of opaline silica and jarosite (Milliken et al., 2008; Metz et al., 2009). The LDs in these two regions may have formed during a common period, the Late Hesperian, and possibly after the LDs located near Juventae and Ganges Chasmata.

Figure 19

Despite these disparities between the LDs of the different regions, LDs display many common geological characteristics that suggest a common geological history. The LDs are composed of consolidated material weaker than the chasmata wall material and are mantled by a dark material that could have been released in situ by erosion of the LDs. Lobate ejecta, pedestal craters, polygonal fractures, valleys and sinuous ridges, and the pitted topographic surface of LDs near Juventae Chasma correspond to morphological features consistent with the occurrence of liquid or solid water in LDs (Table 1). Liquid water originating from precipitation and/or melting of ice contained in the LDs episodically eroded the LDs by fluvial processes during and after their emplacement. The mineralogical composition of the LDs (opaline silica or Al-rich phyllosilicates and hydroxylated ferric oxides) is consistent with the interpretation that LDs result from aqueous alteration of basaltic dust in an acidic environment (possibly alkaline at the beginning of the alteration) probably at low temperatures.

Table 1

5.2 Mode of emplacement and source of the material

The deposition process(es) of the LDs have to be consistent with all the following observations.

(1) LDs occupy a large area of at least 40000 km^2.

(2) LDs are located at various elevations, both on plateaus and in shallow depressions (grabens, craters, pits, hanging depression).

(3) These plateaus are highly elevated ($\geq$1800 m).

(4) LDs are composed of consolidated material weaker than the chasmata wall material.

The mode of emplacement that is most consistent with all the observations is airfall deposition. It accounts for the widespread extent of LDs and their occurrence at various elevations, both in depressions and on plateaus (Table 1). The material consistent with airfall deposition is dust and/or volcanic ash. Tanaka (2000) indicates that large amounts of dust were generated by

impacts, volcanism, and surface processes during the Noachian. LDs can therefore correspond to a dust reservoir accumulated during the Hesperian. Tanaka (2000) also suggested that some Late Hesperian and younger deposits may have resulted from local sources of fine-grained material such as volcanic eruptions. Consequently, LDs can finally result from episodical deposition of remobilized dust (e.g. during dust storms) and ash erupted from the Tharsis Montes, Olympus Mons, Syria Planum shield volcanoes or others volcanic vents in the region.

Even if the mapping of LDs displays some uncertain boundaries, LDs clearly do not cover the whole plateau around Valles Marineris. Considering that LDs consist of an airfall deposition of ash and/or dust material, we can wonder why they are observed near Tithonium, Ius, Candor, Juventae and Ganges Chasmata only. An explanation is that LDs have been deposited above all plateaus and were then massively eroded where they are absent today. However, clues such as remnant buttes would indicate the former presence of LDs on these locations. Another possible explanation is that wind circulations during the Hesperian favoured the accumulation of windblown materials on areas where LDs crop out today. Another hypothesis would be that LDs essentially consist of airfall products of localized volcanic eruptions associated with rifting in Valles Marineris. The last hypothesis we propose is that ash/dust has been preserved from erosion due to cementation by ice. Indeed, current ice distribution maps obtained by climatic modelling at moderate to high obliquity of Mars (e.g., Forget et al., 2007; Madeleine et al., 2009) are remarkably consistent with the current distribution of LDs. Ice (snow precipitation) may have locally cemented ash/dust deposits and form the LDs. Sulfates or other binding agents may have contributed to the cementation of the deposits. Areas where ash/dust received less or no precipitation, and could not cement by percolating fluids, would have been preferentially eroded by eolian processes.

The occurrence of valleys and sinuous ridges in the LDs attests that fluvial activity occurred during the geological history of the LDs (Table 1). The LDs have been eroded, transported, and deposited in fluvial channels, and locally in a lake located in the hanging depression near Melas Chasma. Aerial material may have also contributed to the infilling of the lake.

Weitz et al. (2010) observed light-toned beds within the sinuous ridges near Juventae Chasma and Ganges Chasma, and propose that this is strong evidence that these LDs result from fluvio-lacustrine processes. However, a fluvio-lacustrine origin for most of the LDs is problematic. First of all, the light-toned beds occurring under the top of the sinuous ridges can also be considered as material protected from erosion by the consolidated sinuous ridges, and not as fluvio-lacustrine material. Also, deposition in a plateau-wide lacustrine environment would be inconsistent with the high elevation of the plateau and the area occupied by LDs. Indeed, it would require an unreasonable amount of water to fill lakes (and the associated ground reservoir) at such elevations, and during a substantial period of time to accumulate several tens of meters of sediments. Besides, the absence of topographic basins for most LDs is problematic for a lacustrine hypothesis. The source of the material remains also a problem for this mode of emplacement. In the case of the LDs near Juventae Ganges, and Ius Chasmata, the source of the material deposited is not identifiable. Consequently, this process cannot account for most LDs but cannot be excluded for LDs located in shallow depressions such as the pit near Juventae Chasma and the hanging depression west of Melas Chasma. Therefore we favour the hypothesis that the current LD outcrops result from cycles of emplacement by airfall processes and erosion by fluvial processes.

5.3 The role of ice

Many recent geological studies suggest that ice played a significant role in the geological history of layered deposits on Mars (Tanaka, 2000; Niles and Michalski, 2009; Hynek, 2009).

Tanaka (2000) suggested that deposits of similar scale as the polar ice caps but older may have formed by similar processes in non polar regions including the Medusae Fossae Formation, the Electris deposits (eastern Terra Cimmeria and western Terra Sirenum), the south polar pitted deposits, the Arabia deposits and undivided Noachian materials. These deposits produced by fallout of air-borne dust and precipitation of ice should be fine grained and layered, reflecting cyclic climatic variations. The alternating bright and dark layers (and the associated dark mantle) of LDs may reflect this kind of cyclic variations.

Niles and Michalski (2009) suggest that layered deposits in Terra Meridiani consist of dust and sand captured in a massive ice deposit with volcanic aerosols. Dust and sand particules were weathered into highly hydrated mixtures of siliciclastic and sulphate minerals under acid conditions within the ice. Then, this material would have been reworked by impacts and eolian processes, dehydration, and possibly ice melting. Niles and Michaslski (2009) propose that this kind of ice-weathering model may be relevant for many sediments on Mars.

In the case of LDs, a large amount of ice like an ice cap was not necessarily required to explain the observed morphologies. This is suggested by the mineralogical composition of LDs that is consistent with low water-to-rock ratios (Milliken et al., 2008), and by the sinuous ridges that are interpreted as inverted channels rather than as eskers. Episodical precipitation in regions of LDs may have alimented a substrate enriched in ice. Global events (e.g. obliquity changes) or local events (e.g., impacts, volcanic activity) may have occasionally warmed this permafrost and result in flows of melt waters in LDs. Ice may also have sublimed from LDs. In that case, LDs can be compared to the Dissected Mantle Terrains currently observed in mid- to high latitudes on Mars

(e.g., Mustard et al., 2001; Milliken et al., 2003), which correspond to a mantle of mixed dust and ice that is partially or totally dissected by sublimation.

5.4 Geological history

We propose the following scenario for the geological history of LDs in the region of Valles Marineris:

(1) Deposition of airfall dust and/or volcanic ash on the plateaus.

(2) Imbibition of these deposits by water ice and/or liquid water (coming from precipitation such as rain and snow).

(3) Formation of secondary hydrated minerals (opaline silica or Al-rich phyllosilicates and hydroxylated ferric oxides) in response to aqueous alteration at low temperatures in an acidic environment (possibly alkaline at the beginning of the alteration).

(4) Local fluvial erosion during and after LD deposition.

These four geological events correspond to cyclic events, which probably reflect climatic cycles that reproduced all along the Hesperian Epoch, and possibly the Amazonian Epoch. During these cycles, impacts led to the formation of lobate ejecta blankets, and polygonal fractures were formed. Eolian erosion of LDs is an ongoing process that exhumes buried sinuous ridges.

6. Conclusions

The geological analyses of LDs on the plateaus around Valles Marineris provided the following observations and conclusions.

(1) LDs consist of a series of alternating light and dark beds weaker than the chasmata wall material. They are one hundred meters thick at most and they are covered by a dark unconsolidated erosional lag.

(2) They cover an area of more than 40000 km^2 and are located both on highly elevated plateaus (≥1800 m) and in shallow depressions (grabens, craters, pits, hanging depression).

(3) LDs probably mainly result from airfall deposition of dust and/or volcanic ash.

(4) They were emplaced during the Early to Late Hesperian, and possibly later depending on the region, before the end of the backwasting of the walls near Juventae Chasma, and probably before the formation of Louros Valles by sapping processes near Ius Chasma.

(5) LDs are associated with different morphological features (lobate ejecta and pedestal craters, polygonal fractures, valleys and sinuous ridges, a pitted surface) that are consistent with the presence of interstitial liquid water and/ or water ice (originating from precipitation) during and after their deposition.

(6) LDs were episodically eroded by fluvial processes. The fluvial erosion of LDs locally resulted in the formation of lacustrine deposits in the hanging depression south of Melas Chasma.

(7) LDs probably consisted of layers of airfall dust and/or ash mixed with ice particles, and hence can be associated to pristine Dissected Mantle Terrains developed at a period when the ice was stable in the subsurface in the equatorial regions.

(8) The spectral characteristics of LDs attest to aqueous alteration in an acidic environment (possibly alkaline at the beginning of the alteration) probably at low temperatures.

(9) The alternating bright and dark layers of LDs may reflect a climatic cycle of ice stability and ice thawing/sublimation associated to fluvial episodes and to alteration processes in airfall layered deposits during the Hesperian, and possibly the Amazonian.

Aknowledgements

We greatly appreciated fruitful discussions about this study with N. Mangold, C. Quantin-Nataf, P. Allemand, and J. Flahaut. We would like to thank J. L. Bishop and an anonymous reviewer for

their relevant comments and suggestions that greatly improved the manuscript. Thank you to the MRO HiRISE and CRISM teams for the powerful resources available on the web. This research has been supported by the Programme National de Planétologie (Institut National des Sciences de l'Univers, INSU, CNRS), by the French Ministry of Higher Education and Research, by the Centre National d'Études Spatiales (CNES) and by the Helmholtz Association through the research alliance "Planetary Evolution and Life".

References

Anderson J.H., and K. A. Wickersheim (1964), Near infrared characterization of water and hydroxyl groups on silica surfaces, *Surface Science*, 2, 252-260.

Banerjee, I, and B. C. McDonald (1975), Nature of Esker sedimentation, Glaciofluvial and glaciolacustrine sedimentation Soc. Econ. Paleontol. Mineral. Spec. Publ., A. V. Jopling and B. C. McDonald Ed., 23:132-154.

Baratoux, D., N. Mangold, P. Pinet, and F. Costard (2005), Thermal properties of lobate ejecta in Syrtis Major, Mars: Implications for the mechanisms of formation, *J. Geophys. Res., 110*(E4), E04011, doi:10.1029/2004JE002314.

Barlow, N. G. (2005), A New Model for Pedestal Crater Formation, *Workshop on the Role of Volatiles and Atmospheres on Martian Impact Craters*, Laurel, Maryland, Abstract 3041.

Barnouin-Jha, O. S., and P. H. Schultz (1996), *Ejecta entrainment by impact-generated ring vortices: Theory and experiments*, *J. Geophys. Res., 101*(E9), 21,099–21,115.

Barnouin-Jha, O. S., P. H. Schultz and J. H. Lever (1999a), Investigating the interactions between an atmosphere and an ejecta curtain 1. Wind tunnel tests, *J. Geophys. Res., 104* (E11), 27,105-27,115.

Barnouin-Jha, O. S., P. H. Schultz, and J. H. Lever (1999b) Investigating the interactions between an atmosphere and an ejecta curtain 2. Numerical experiments, *J. Geophys. Res.*, 104 (E11), 27,117-27,131.

Beyer, R. A., and A. S. McEwen (2005), Layering stratigraphy of eastern Coprates and northern Capri Chasmata, Mars, *Icarus, 179*(1), 1-23, doi:10.1016/j.icarus.2005.06.014.

Bibring, J.-P., A. Soufflot, M. Berthé, Y. Langevin, B. Gondet, P. Drossart, M. Bouyé, M. Combes, P. Puget, A. Semery, G. Bellucci, V. Formisano, V. Moroz, V. Kottsov, G. Bonello, S. Erard, O. Forni, A. Gendrin, N. Manaud, F. Poulet, G. Poulleau, T. Encrenaz, T. Fouchet, R. Melchiori, F. Altieri, N. Ignatiev, D. Titov, L. Zasova, A. Coradini, F. Capacionni, P. Cerroni, S. S. Fonti, N. Mangold, P. Pinet, B. Schmitt, C. Sotin, E. Hauber, H. Hoffmann, R. Jaumann, U. Keller, R. Arvidson, J. Mustard, and F. Forget (2004), OMEGA: Observatoire pour la Minéralogie, l'Eau, les Glaces et l'Activité, In: *Mars Express: The Scientific Payload*, edited by A. Wison, *Eur. Space Agency Spec. Publ., 1240,* 37–49.

Bishop, J. L., M. Parente, C. M. Weitz, E. Z. Noe Dobrea, W. M. Calvin, R. E. Milliken, L. H. Roach, S. L. Murchie, N. K. McKeown, J. F. Mustard, and The Crism Team (2008),

Characterization of Light-toned Sulfate and Hydrated Silica Layers at Juventae Chasma Using CRISM, OMEGA, HiRISE and CTX Images, *Lunar Planet. Sci., XXXIX*, Abstract 2334.

Bishop, J. L., M. Parente, C. M. Weitz, E. Z. Noe Dobrea, L. H. Roach, S. L. Murchie,, P. C. McGuire, N. K. McKeown, C. M. Rossi, A. J. Brown, W. M. Calvin, R. E. Milliken, J. F. Mustard (2009), Mineralogy of Juventae Chasma: Sulfates in he Light-toned Mounds, Mafic Minerals in the Bedrock, and Hydrated Silica and Hydroxylated Ferric Sulfate on the Plateau, *J. Geophys. Res., 114*, E00D09, doi:10.1029/2009JE003352.

Carr, M. H., L. Crumpler, J. Cutts, R. Greeley, J. Guest, and H. Masursky (1977), Martian impact craters and emplacement of ejecta by surface flow, *J. Geophys. Res., 82*, 4055–4065.

Catling, D. C., S. E. Wood, C. Leovy, D. R. Montgomery, H. M. Greenberg, C. R. Glein, and J. M. Moore (2006), Light-toned layered deposits in Juventae Chasma, Mars, *Icarus, 181*(1), 26-51, doi:10.1016/j.icarus.2005.10.020.

Clark R. N. et al. (2007) USGS splib06a: U.S. Geological Survey, Digital Data Series 231.

Christensen, P.R., N.S. Gorelick, G.L. Mehall, and K.C. Murray, *THEMIS Public Data Releases*, Planetary Data System node, Arizona State University, <http://themis-data.asu.edu>.

Coleman, N. M., C. L. Dinwiddie, and K. Casteel (2007), High outflow channels on Mars indicate Hesperian recharge at low latitudes and the presence of Canyon Lakes, *Icarus, 189*(2), 344-361 doi: 10.1016/j.icarus.2007.01.020.

Desborough, G. A., K. S. Smith, H. A. Lowers, G. A. Swayze, J. M. Hammarstrom, S. F. Diehl, R. L. Driscoll, and R. W. Leinz (2006), The use of synthetic jarosite as an analog for natural jarosite, paper presented at Proceedings of the Seventh International Conference on Acid Rock Drainage (ICARD 7), St. Louis, Missouri, March 26-30, 2006.

Evans, D. (2005), Ice-marginal terrestrial landsystems: active temperate glacier margins, In Evans D (Ed.) Glacial Landsystems. Hodder Arnold, London, p. 12- 43.

Forget, F., F. Montmessin, B. Levrard, R. M. Haberle, J. W. Head, and J.-B. Madeleine (2007), Glaciers, Polar Caps and Ice Mantling: The Effect of Obliquity on Martian Climate, in *Seventh International Conference on Mars,* Abstract 3028.

Hurowitz, J.A., McLennan, S.M., Lindsley, D.H., and Schoonen, M.A. (2005), Experimental epithermal alteration of synthetic Los Angeles meteorite: Implications for the origin of Martian soils and identifi cation of hydrothermal sites on Mars, *J. Geophys. Res.*, *110,* E07002, doi: 10.1029/2004JE002391.

Kadish, S. J., and N. G. Barlow (2006), Pedestal Crater Distribution and Implications for a New Model of Formation, *Lunar Planet. Sci., XXXVII*, Abstract 1254.

Kadish, S. J., J. W. Head, and N. G. Barlow (2008), Pedestal Craters on Mars: Distribution, Characteristics, and Implications for Amazonian Climate Change, *Lunar Planet. Sci., XXXIX*, Abstract 1766.

Kadish, S. J., J. W. Head, and N. G. Barlow (2009), Mid-Latitude Pedestal Crater heights: A Proxi for the Thickness of a Past Climate-Related, Ice-Rich Substrate, *Lunar Planet. Sci., XXXX*, Abstract 1313.

Kochel, R.C., Piper, J. (1986), Morphology of large valleys on Hawaii: evidence for ground water sapping and comparisons with Martian valleys, *J. Geophys. Res., 91,* E171–E192.

Le Deit, L., O. Bourgeois, S. Le Mouélic, D. Mège, J.-Ph. Combe, C. Sotin, M. Massé (2008a), Light-Toned Layers on Plateaus above Valles Marineris (Mars), *Lunar Planet. Sci., XXXIX*, Abstract 1740.

Le Deit, L., O. Bourgeois, S. Le Mouélic, C. Quantin-Nataf, D. Mège, C. Sotin, M. Massé, V. Sarago (2008b), Morphology, composition, age and spatial extent of a layered superficial formation covering the plains around Valles Marineris, Mars, *European Planetary Science Congress*, abstract 327.

Le Deit, L., S. Le Mouélic, O. Bourgeois, D. Mège, M. Massé, C. Quantin-Nataf, C. Sotin, J.-P. Bibring, B. Gondet, Y. Langevin (2008c), Composition and Morphology of Hydrated Layered Deposits on the Plains around Valles Marineris (Mars), *Martian Phyllosilicates: Recorders of Aqueous Processes?*, abstract 7016.

Le Deit, L., O. Bourgeois, D. Mège, S. Le Mouélic, M. Massé, E. Hauber, R. Jaumann, J.-P. Bibring (2009), Geological History of a Light-toned Formation Draping the Plateaus in the Region of Valles Marineris, *Lunar Planet. Sci. Conf., XXXX*, abstract#1856.

Laity, J. E., M. C. Malin (1985), Sapping processes and the development of theatre-headed valley networks on the Colorado Plateau, *Geol. Soc. of Am. Bull., v. 96*, p. 203-217.

Langevin, Y., F. Poulet, J.-P. Bibring, and B. Gondet (2005), Sulfates in the north polar region of Mars detected by OMEGA/Mars Express, *Science, 307*(5715), 1584–1586.

Lefort, A., P. S. Russell, N. Thomas, A. S. McEwen, C. M. Dundas, R. L. Kirk (2009), Observations of periglacial landforms in Utopia Planitia with the High Resolution Imaging Science Experiment (HiRISE), *J. Geophys. Res., 114*, E04005, doi:10.1029/2006JE003264.

Loizeau, D., N. Mangold, F. Poulet, J.-P. Bibring, A. Gendrin, V. Ansan, C. Gomez, B. Gondet, Y. Langevin, P. Masson, and G. Neukum (2007), Phyllosilicates in the Mawrth Vallis region of Mars, *J. Geophys. Res., 112*(E8), E08S08, doi:10.1029/2006JE002877.

Lucchitta, B. K., A. S. McEwen, G. D. Clow, P. E. Geissler, R. B. Singer, R. A. Schultz, and S. W. Squyres (1992), The canyon system on Mars, in *Mars, Univ. of Arizona*, Tucson, 453–492.

Lucchitta, B. K. (2005), Light Layer and Sinuous Ridges on Plateau Near Juventae Chasma, Mars, *Lunar Planet. Sci., XXXVI*, Abstract 1500.

Madeleine, J.-B., F. Forget, J. W. Head, B. Levrard, F. Montmessin, E. Millour (2009), Amazonian Northern Mid-Latitude Glaciation on Mars: A Proposed Climate Scenario, *Icarus*, in press.

Malin, M. C., M. H. Carr, G. E. Danielson, M. E. Davies, W. K. Hartmann, A. P. Ingersoll, P. B. James, H. Masursky, A. S. McEwen, L. A. Soderblom, P. Thomas, J. Veverka, M. A. Caplinger, M. A. Ravine, T. A. Soulanille, and J. L. Warr En (1998), Early Views of the Martian Surface from the Mars Orbiter Camera of Mars Global Surveyor, *Science, 279*(5357), 1681.

Malin, M. C., and K. S. Edgett (2000), Sedimentary Rocks of Early Mars, *Science, 290*(5498), 1927-1937.

Malin, M. C., J. F. Bell, B. A. Cantor, M. A. Caplinger, W. M. Calvin, R. Clancy, E. T., K. S. Edgett, L. Edwards, R. M. Haberle, P. B. James, S. W. Lee, M. A. Ravine, P. C. Thomas, and M. J. Wolff (2007), Context Camera Investigation on board the Mars Reconnaissance Orbiter, *J. Geophys. Res., 112*(E5), E05S04, doi:10.1029/2006JE002808.

Mangold, N. (2005), High latitude patterned grounds on Mars: Classification, distribution and climatic control, *Icarus, 174*, 336-359.

Mangold, N., V. Ansan, Ph. Masson, C. Quantin, and G. Neukum (2008), Geomorphic study of fluvial landforms on the northern Valles Marineris plateau, Mars, *J. Geophys. Res., 113*(E8), E08009, doi:10.1029/2007JE002985.

McCauley, J. F. (1973), Mariner 9 evidence for wind erosion in equatorial and mid-latitude regions of Mars, *J. Geophys. Res., 78*,4123-4138.

McEwen, A. S., M. C. Malin, M. H. Carr, and W. K. Hartmann (1999), Voluminous volcanism on early Mars revealed in Valles Marineris, *Nature, 397,* 584– 586, doi:10.1038/17539.

McEwen, A. S., E. M. Eliason, J. W. Bergstrom, N. T. Bridges, C. J. Hansen, W. A. Delamere, J. A. Grant, V. C. Gulick, K. E. Herkenhoff, L. Keszthelyi, R. L. Kirk, M. T. Mellon, S. W. Squyres, N. Thomas, and C. M. Weitz (2007), Mars Reconnaissance Orbiter's High Resolution Imaging Science Experiment (HiRISE), *J. Geophys.Res., 112*(E5), E05S02, doi: 10.1029/2005JE002605.

Metz, J. M., J. P. Grotzinger, D. Mohrig, R. Milliken, B. Prather, C. Pirmez, A. S. McEwen, and C. M. Weitz (2009), Sublacustrine depositional fans in southwest Melas Chasma, *J. Geophys. Res.*, 114, E10002, doi:10.1029/2009JE003365.

Milliken, R. E., J. F. Mustard, and D. L. Goldsby (2003), Viscous flow features on the surface of Mars: Observations from high-resolution Mars Orbiter Camera (MOC) images, *J. Geophys. Res., 108*(E6), 11-1, 5057, doi: 10.1029/2002JE002005.

Milliken, R. E., G. Swayze, S. Murchie, J. Bishop, R. Clark, B. Ehlmann, J. Grotzinger, J. Mustard, and C. Weitz (2007), Spectral Evidence for Aqueous Alteration of the Plains Surrounding Valles Marineris, Mars, *AGU, Fall Meet.*, Abstract P12A-02.

Milliken, R. E., G. A. Swayze, R. E. Arvidson, J. L. Bishop, R. N. Clark, B. L. Ehlmann, R. O. Green, J. P. Grotzinger, R. V. Morris, S. L. Murchie, J. F. Mustard, C. M. Weitz (2008),

Opaline Silica in young deposits on Mars, *Geology, v. 36,* no. 11, p. 847-850, doi:10.1130/G24967A.1.

Morgenstern, A., E. Hauber, D. Reiss, S. van Gasselt, G. Grosse, L. Schirrmeister (2007), Deposition and degradation of a volatile-rich layer in Utopia Planitia and implications for climate history on Mars, *J. Geophys. Res., 112*, E06010, doi:10.1029/2006JE002869..

Morris, R. V., D. C. Golden, D. W. Ming, T. G. Graff, R. E. Arvidson, S. M. Wiseman, and K. A. Lichtenberg (2009), Visible and near-IR reflectance spectra for smectite, sulfate and perchlorate under dry conditions for interpretation of martian surface mineralogy, *Lunar Planet. Sci., XXXX,* Abstract 2317.

Mouginis-Mark, P. (1979), Martian fluidized crater morphology - Variations with crater size, latitude, altitude, and target material, *J. Geophys. Res., 84*, 8011-8022.

Murchie, S., R. Arvidson, P. Bedini, K. Beisser, J.-P. Bibring, J. Bishop, J. Boldt, P. Cavender, T. Choo, R. T. Clancy, E. H. Darlington, D. Des Marais, R. Espiritu, D. Fort, R. Green, E. Guinness, J. Hayes, C. Hash, K. Heffernan, J. Hemmler, G. Heyler, D. Humm, J. Hutcheson, N. Izenberg, R. Lee, J. Lees, D. Lohr, E. Malaret, T. Martin, J. A. McGovern, P. McGuire, R. Morris, J. Mustard, S. Pelkey, E. Rhodes, M. Robinson, T. Roush, E. Schaefer, G. Seagrave, F. Seelos, P. Silverglate, S. Slavney, M. Smith, W.-J. Shyong, K. Strohbehn, H. Taylor, P. Thompson, B. Tossman, M. Wirzburger, and M. Wolff (2007), Compact

reconnaissance imaging spectrometer for Mars (CRISM) on Mars Reconnaissance Orbiter (MRO), *J. Geophys. Res., 112*(E5), E05S03, doi:10.1029/2006JE002682.

Murchie, S. L., J. F.Mustard, B. L. Ehlmann, R. E. Milliken, J. L Bishop., N. K McKeown, E. Z. Noe Dobrea, F. P. Seelos, D. L. Buczkowski, S. M. Wiseman, R. E Arvidson, J. J.Wray, G. A. Swayze, R. N.Clark, D. J.Des Marais, A. S. McEwen, J.-P. Bibring (2009a) A synthesis of Martian aqueous mineralogy after 1 Mars year of observations from the Mars Reconnaissance Orbiter, *J. Geophys. Res., 114***,** doi:10.1029/2009JE003342.

Murchie, S. L., F. P. Seelos, C. D. Hash, D. C. Humm, E. Malaret, J. A. McGovern, T. H. Choo, K. D. Seelos, D. L. Buczkowski, M. F. Morgan, O. S. Barnouin-Jha, H. Nair, H. W. Taylor, G. W. Patterson, C. A. Harvel, J. F. Mustard, R. E. Arvidson, P. McGuire, M. D Smith, M. J. Wolff, T. N. Titus, J.-P. Bibring, F. Poulet (2009b), The Compact Reconnaissance Imaging Spectrometer for Mars investigation and data set from the Mars Reconnaissance Orbiter's primary science phase, *J. Geophys. Res., 114***,** doi:10.1029/2009JE003344.

Hynek, B. (2009), Ancient equatorial ice on Mars ?, *Nature Geosci., 2*, 215–220.

Mustard, John F., C. D. Cooper, and M. K. Rifkin (2001), Evidence for recent climate change on Mars from the identification of youthful near-surface ground ice, *Nature, 412*(6845), 411-414.

Mustard, J. F., S. L. Murchie, S. M. Pelkey, B. L. Ehlmann, R. E. Milliken, J. A. Grant, J.-P. Bibring, F. Poulet, J. Bishop, E. Noe Dobrea ; L. Roach, F. Seelos, R. E. Arvidson, S. Wiseman, R. Green, C. Hash, D. Humm, E. Malaret, J. A. McGovern, K. Seelos, T. Clancy, R.

Clark, D. D. Marais, N. Izenberg, A. Knudson, Y. Langevin, T. Martin, P. McGuire, R. Morris, M. Robinson, T. Roush, M. Smith, G. Swayze, H. Taylor, T. Titus, and M. Wolff (2008), Hydrated silicate minerals on Mars observed by the Mars Reconnaissance Orbiter CRISM instrument, *Nature, 454*(7202), 305-309, doi: 10.1038/nature07097.

Nedell, S. S., S. W. Squyres, and D. W. Andersen (1987), Origin and evolution of the layered deposits in the Valles Marineris, Mars, *Icarus, 70*, 409-441, doi: 10.1016/0019-1035(87)90086-8.

Neukum, G., and R. Jaumann (2004), HRSC: The high resolution stereo camera of Mars express, in *Mars Express: The Scientific Payload, ESA SP-1240*, pp. 17-35.

Niles, P. B., and J. Michalski (2009), Meridiani Planum sediments on Mars formed through weathering in massive ice deposits, *Nature Geosci., 2*, 215–220.

Peulvast, J. P., D. Mège, J. Chichiak, F. Costard and Ph. L. Masson (2001), Morphology, evolution and tectonics of Valles Marineris wallslopes (Mars), *Geomorphology*, *37*(3-4), 329-352, doi: 10.1016/S0169-555X(00)00085-4.

Phillips, R. J., M. T. Zuber, S. C. Solomon, M. P. Golombek, B. M. Jakosky, W. B. Banerdt, D. E. Smith, R. M. E. Williams, B. M. Hynek, O. Aharonson, and S. A. Hauck (2001), Ancient Geodynamics and Global-Scale Hydrology on Mars, *Science, 291*(5513), 2587-2591.

Putzig, N. E., M. T. Mellon (2007), Apparent thermal inertia and the surface heterogeneity of Mars, *Icarus, 191,* 68-94, doi: 10.1016/j.icarus.2007.05.013.

Quantin, C., P. Allemand, N. Mangold, G. Dromart, and C. Delacourt (2005a), Fluvial and lacustrine activity on layered deposits in Melas Chasma, Valles Marineris, Mars, *J. Geophys. Res., 110*(E12), E12S19, doi:10.1029/2005JE002440.

Rapp, A. and G. M. Clark, (1971), Large nonsorted polygons in Padjelanta National Park, Swedish Lappland, Geografiska Annaler, 53A, pp.71-85.

Roach, L. H., J. F. Mustard, G. A. Swayze, R. Milliken, J. L. Bishop, S. L. Murchie (2010), Hydrated Mineral Stratigraphy of Ius Chasma, Valles Marineris, *Icarus*, in press.

Schultz, P. H., and D. E. Gault (1979), Atmospheric effects on Martian ejecta emplacement, *J. Geophys. Res., 84(B13)*, 7669–7687.

Scott, D, and M. Carr (1978), Geological Map of Mars, 1:25.000.000. Reston, VA, U.S. Geological Survey Technical Report (Miscellaneous Investigation Series).

Scott, D. H., and K. L. Tanaka (1986), Geologic Map of the western equatorial region of Mars. *U. S. Geol. Survey Misc.* Map I-1802-A.

Seidelmann, P. K., V. K. Abalakin, M. Bursa, M. E. Davies, C. de Bergh, J.H. Lieske, J. Oberst, J. L. Simon, E. M. Standish, P. Stooke, and P. C. Thomas (2002), Report of the IAU/IAG

working group on cartographic coordinates and rotational elements of the planets and satellites: 2000, *Celestial Mech. Dyn. Astron., 82*, 83–110.

Segura, T. L., O. B. Toon, A. Colaprete, K. Zahnle (2002), Environmental Effects of Large Impacts on Mars, *Science, 298* (5600), 1977-1980.

Smith, D. E., M. T. Zuber, H. V. Frey, J. B. Garvin, J. W. Head, D. O. Muhleman, G. H. Pettengill, R. J. Phillips, S. C. Solomon, H. J. Zwally, W. B. Banerdt, T. C. Duxbury, M. P. Golombek, F. G. Lemoine, G. A. Neumann, D. D. Rowlands, O. Aharonson, P. G. Ford, A. B. Ivanov, C. L. Johnson, P. J. McGovern, J. B. Abshire, R. S. Afzal, and X. Sun (2001), Mars Orbiter Laser Altimeter (MOLA): Experiment summary after the first year of global mapping of Mars, *J. Geophys. Res.*, *106*(E10), 23,689– 23,722, doi:10.1029/2000JE001364.

Stoffregen, R.E., Alpers, C.N., and Jambor, J.L. (2000), Alunite-jarosite crystallography, thermodynamics, and geochronology, *in* Alpers, C., et al., eds., Sulfate minerals: Crystallography, geochemistry, and environmental significance: Mineralogical Society of America Reviews in Mineralogy and Geochemistry, v. 40, p. 453–479.

Squyres, S. W., A. H. Knoll, R. E. Arvidson, B. C. Clark, J. P. Grotzinger, B. L. Jolliff, S. M. McLennan, N. Tosca, J. F. Bell III, W. M. Calvin, W. H. Farrand, T. D. Glotch, M. P. Golombeck, K. E. Herkenhoff, J. R. Johnson, G. Klingelhofer, H. Y. McSween, A. S. Yen (2006), Two Yearsat Meridiani Planum: Results from the Opportunity Rover, *Science, 313* (5792), 1403-1407.

Swayze, G. A., R. E. Milliken, R. N. Clark, J. L. Bishop, B. L. Ehlmann, S. M. Pelkey, J. F. Mustard, S. L. Murchie, A. J. Brown, and The MRO CRISM Team (2007), Spectral Evidence for Hydrated Volcanic and/or Impact Glass on Mars with MRO CRISM, in *7th International Conference on Mars*, Abstract 3384.

Tanaka K. L. (2000), Dust and Ice Deposition in the Martian Geologic Record, *Icarus, 144*, 254-266, doi:10.1006/icar.1999.6297.

Treiman, A. H., K. H. Fuks, and S. Murchie (1995), Diagenetic layers in the upper walls of Valles Marineris, Mars: Evidence for drastic climate change since the mid-Hesperian, *J. Geophys. Res., 100*(E12), 26339-26344, doi:10.1029/95JE03223.

Tosca, N. J., S. M. McLennan, D. H. Lindsley, and M. A. A. Schoonen (2004), Acid-sulfate weathering of synthetic Martian basalt: The acid fog model revisited, *J. Geophys. Res., 109*, E05003, doi:10.1029/ 2003JE002218.

Weitz, C. M., R. E. Milliken, J. A. Grant, A. S. McEwen, R. M. E. Williams, J. L. Bishop (2008), Light-toned strata and inverted channels adjacent to Juventae and Ganges chasmata, Mars, *Geophys. Res. Letters, 35*, L19202, doi:10.1029/2008GL035317.

Weitz, C. M., R. E. Milliken, J. A. Grant, A. S. McEwen, R. M. E. Williams, J. L. Bishop and B. J. Thomson (2010), Mars Reconnaissance Orbiter observations of light-toned layered deposits and associated fluvial landforms on the plateaus adjacent to Valles Marineris, *Icarus, 205***,** 73-102, doi:10.1016/j.icarus.2009.04.017.

Williams, J. P., D. A. Paige, and C. E. Manning (2003), Layering in the wall rock of Valles Marineris: intrusive and extrusive magmatism, *Geophys. Res. Lett.*, *30*(12), 1623, 25-1, doi:10.1029/2003GL017662.

Williams, R. M. E., M. C. Malin, K. S. Edgett (2005), Remnants of the courses of fine-scale, precipitation-fed runoff streams preserved in the martian rock record, *Lunar Planet. Sci., XXXVI,* Abstract 1173.

Williams, R. M. E., C. M. Weitz (2009), Stratigraphic context for inverted channels on the plains north of Juventae Chasma: Implications for post-Noachian martian climate change, *Lunar Planet. Sci., XXXX,* Abstract 1935.

Witbeck, N. E., K. L. Tanaka, and D. H. Scott (1991), Geologic map of the Valles Marineris region, Mars, *U.S. Geol. Surv. Misc. Invest. Ser*., Map I-2010.

Table caption

Table 1: List summarizing the observations supporting the geological processes that have affected the LDs and their implications.

Figure captions

Figure 1: Layered deposits (LDs) cropping out on Lunae Planum southwest of Juventae Chasma. (a) Subset of HRSC color image (orbit 243). Location of (b) and (c) is indicated. (b) Subset of HiRISE grayscale image (PSP_003579_1755) displaying LDs draping the Lunae Planum basement. LDs are overlain by a dark mantle. (c) Subset of HiRISE IRB color image (PSP_003579_1755) showing LDs close to the Juventae Chasma wall.

Figure 2: Location of LDs (orange patches) on plateaus above Valles Marineris (THEMIS IR daytime mosaic superimposed on a MOC mosaic). Boundaries where LDs are not clearly defined are dashed. Locations of Figures 3, 6, and 8 are marked.

Figure 3: LDs south of Ius Chasma. (a) THEMIS IR daytime mosaic. (b) Morphological map of LDs (orange) superimposed on (a). (c) THEMIS IR nighttime mosaic in color superimposed on the THEMIS IR daytime mosaic. The brightness temperature of terrains at night is displayed from blue to red. The warmest ones are red. White arrows indicate fresh outcrops of LDs that are warmer than LDs' surface and surrounding plateau. (d) Interpretative section across the plateau (topographic profile drawn from MOLA grid at 128 pix/deg located on (a), (b), and (c)).

Figure 4: Valleys carved in LDs and connected to the heads of Louros Valles. Portion of CTX image P15_006797_1725.

Figure 5: Close-up views of LDs in the hanging depression southwest of Melas Chasma. (a) Mosaic of CTX images showing the hanging depression filled with LDs, which are eroded by valley networks visible in (d), and lacustrine deposits located in an enclosed depression (see Quantin et al., 2005 for more details). Stars indicate the location of delta deposits. Elevation contours (interval 200 m) extracted from MOLA DEM are displayed. The Hesperian plateau corresponds to units Hr and Hsu of Witbeck et al. (1991). (b) CTX image (P05_002907_1706) showing the eastern border of the hanging depression. The main and deep part of Melas Chasma is filled in with ILDs (bottom of the image). LDs cover the basement outcrop (plateau). (c) Portion of HiRISE image (PSP_005663_1700) showing LDs filling the hanging depression. (d) Portion of HiRISE (PSP_009025_1705) image showing LDs incised by valley networks. Illumination from the northwest.

Figure 6: LDs southwest of Juventae Chasma. (a) THEMIS IR daytime mosaic. (b) Morphological map of LDs (orange) and ILDs (light purple) superimposed on (a). Remnant buttes, pedestal craters, sinuous ridges, wrinkle ridges, and the estimated previous lateral extent of LDs (gray) are indicated. (c) THEMIS IR nighttime mosaic in color superimposed on the THEMIS IR daytime mosaic. The brightness temperature of terrains at night is displayed from blue to red. The warmest ones are red. LDs' surface is colder (blue to green) than plateau's surface (green to red). (d) Interpretative section across the plateau (topographic profile drawn from MOLA PEDR (ap11089), which is located on (a), (b), and (c)). The superficial material displayed on the cross-section does not refer to the dark mantle on the LDs, which is not represented here, as the basal layer of the LDs that is presented in the section 4.2.

Figure 7: Portion of Juventae Chasma southern wall displaying a tilted wall block. (a) Portion of CTX image (P03_002234_1761). (b) Close-up view of the tilted basement block mantled by LDs (HiRISE ESP_011688_1760). (c) Elevation contours (interval 200 m) extracted from MOLA DEM superposed on (b). LDs were deposited before the tilting of the block, hence before the end of the backward erosion of the walls.

Figure 8 : LDs west of Ganges Chasma. (a) THEMIS IR daytime mosaic. (b) Morphological map of LDs (orange). The Noachian basement (Npl2, green), the ejecta blanket (yellow), the superficial material filling impact craters (light brown) and sinuous ridges (red) are indicated. The outflow channel Allegheny Vallis and the "Scablands" are also reported. (c) THEMIS IR nighttime mosaic in color superimposed on the THEMIS IR daytime mosaic. The brightness temperature of terrains at night is displayed from blue to red. The warmest ones are red. LDs' surface is colder (blue to green) than plateau's surface (green to red). (d) Interpretative section across the plateau (topographic profile drawn from MOLA PEDR (ap20211), which is located on (a), (b), and (c)). The hydrated basal layer is detailed in part 4.2 and is not reported on (b).The superficial material displayed on the cross-section does not refer to the dark mantle on the LDs, which is not represented here.

Figure 9: Histogram showing the average thermal inertia value (TES) in each region of LDs, and the corresponding surface area of each region of LDs. The average thermal inertia value for each region of LDs is based on the map made by Putzig et al. (2007).

Figure 10: An impact crater with lobate ejecta (a, b) and a pedestal impact crater (c, d) near Ganges Chasma. (a) Portion of CTX image (P01_001429_1720) showing lobate ejecta blanket

stratigraphically above LDs. (b) Interpretative sketch map of (a). (c) Portion of CTX image (P01_001429_1720) showing LDs preserved under the ejecta of an impact crater that forms a pedestal. (d) Interpretative sketch map of (c).

Figure 11: Polygons on LD layers near Juventae Chasma (a) and near Ius Chasma (b). (a) Portion of HiRISE image PSP_003579_1755 (image centre: -4.7°N, 296.4°E). (b) Portion of HiRISE image PSP_002459_1715 (image centre: -8.3°N, 275. 2°E).

Figure 12: Valleys carved in LDs (a) and in Hesperian basement (b) near Juventae Chasma. (a) Portion of CTX image P03_002234_1761 displaying a low order valley network incised in LDs. (b) Close view of HiRISE image PSP_005346_1755 in grey scale and in IRB color displaying valleys incised in the Hesperian basement (blue on the color image). Valleys are locally filled in by sinuous ridges (yellow on the color image), which are hence younger than the valleys.

Figure 13: Sinuous ridges associated to LDs near Juventae Chasma. (a) Portion of CTX image P01_001337_1757 showing a dendritic network of sinuous ridges, a wrinkle ridge and pedestal craters. Location of (b) and (c) is indicated. (b) Close-up view of (a) showing a sinuous ridge whose morphology reminds that of abandoned meanders. (c) Portion of HiRISE image PSP_006770_1760 showing a sinuous ridge embedded in LDs. (d) Portion of CTX image P03_002234_1761 displaying linear networks of sinuous ridges located along the border of LDs. Location of (e) and Figure 14 is indicated. (e) Subset of HiRISE image PSP_008853_1760 showing a linear network of sinuous ridges trending NE-SW.

Figure 14: Formations displaying pitted textures. (a) Portion of HiRISE image (PSP_007930_2310) showing a view of Dissected Mantle Terrain (DMT) and scalloped pits in the Tempe Terra region (50.5°N, 295.5°E). The DMT corresponds to a layer of dust mixed with ice (e.g., Milliken et al., 2003). Scalloped pits are thought to be related to the removal of interstitial ice by sublimation (e.g., Morgenstern et al., 2007; Lefort et al., 2009). (b) Portion of CTX image (P03_002234_1761) showing LDs and its pitted texture near Juventae Chasma (-3.8°N, 297.4°E, located on Figure 13). Pits correspond to erosion features, the morphology of which reminds that of sublimation pits showed on (a).

Figure 15: LDs resting on the Noachian plateau west of Ganges Chasma (CRISM cube FRT 8949 superimposed on a mosaic of CTX images). The location of Figure 16a-b is indicated by a white box.

Figure 16: Spectral properties and location of a hydrated layer of LDs near Ganges Chasma. (a) Subset of HiRISE image PSP_005939_1720. Bright outcrops with hydrated signatures are shown (white arrows). (b) Subset of CRISM image FRT 8949 of the LDs. Colored pixels correspond to the location of averaged spectra shown in (c). (c) Spectrum, average spectra overlain by smoothed spectra for CRISM spectra (colored areas) and ratio spectra (division by an average spectrum of spectrally featureless surfaces) of the LDs. (d) Portion of HiRISE IRB color image (PSP_005939_1720, centre of the image: 52.2°W - 8°S) displaying the hydrated basal layer.

Figure 17: Comparison of ratio spectra of LDs with library spectra. Top: CRISM ratio spectra of LDs near Juventae Chasma (FRT 5814), Ganges Chasma (Figure 16) and Melas Chasma (HRL

44ac) (overlain by smoothed ratios). Bottom: USGS library spectra (Clark et al., 2007) and a linear mixture of spectra of montmorillonite and jarosite (50% each).

Figure 18: Views of LD series near Juventae Chasma (a) and Ganges Chasma (b) displaying in the stratigraphic order, the plateau (basement), the basal layer, and the main sequence of LDs. (a) Portion of HiRISE IRB color PSP_003579_1755 (centre of the view: 63.6°W, -4.7°N). (b) Portion of HiRISE IRB color PSP_005161_1720 (centre of the view: 52.7°W, -8.1°N).

Figure 19: Stratigraphic logs of the LDs near Juventae Chasma (a), Ganges Chasma (b), Ius Chasma (c), and in the hanging depression near Melas Chasma (d) summarizing their main morphologic, stratigraphic, and mineralogic properties. Red features represent sinuous ridges, and the v-shaped features represent the valleys. The possible emplacement age of LDs is indicated by gray boxes (N: Noachian; EH: Early Hesperian; MH: Mid-Hesperian; LH: Late Hesperian; A: Amazonian).

Table 1

Aqueous environment / geological processes	Observations	Implications
Aqueous environment	▪ Valleys and sinuous ridges ▪ Lobate ejecta and pedestal craters ▪ Polygonal fractures ▪ Pitted texture ▪ Hydrated minerals (opaline silica and/or Al-phyllosilicate overlain by hydroxylated ferric sulfate)	▪ Possible ice-rich substrate and sublimation ▪ Liquid water originating from precipitation and/or melting of ground ice ▪ Alteration of basaltic material at low temperature ▪ Alkaline to acidic aqueous alteration.
Airfall deposition	▪ Large area of at least 40000 km^2 ▪ Various elevations, both on plateaus and in shallow depressions ▪ Plateaus are highly elevated ($\geq$1800 m) ▪ LDs are composed of consolidated material weaker than the chasmata wall material	▪ Airfall deposition accounts for most of LDs ▪ Fine-grained material such as dust or volcanic ash
Fluvial activity	▪ Valleys ▪ Sinuous ridges	▪ Fluvial erosion and transport of LDs ▪ Fluvial deposition in fluvial channels
Lacustrine deposition	▪ Delta deposits and subhorizontal layers in an enclosed depression at the outlet of valley networks near Melas Chasma	▪ Deposition of the erosion products of LDs in a lake near Melas Chasma

Figure 13

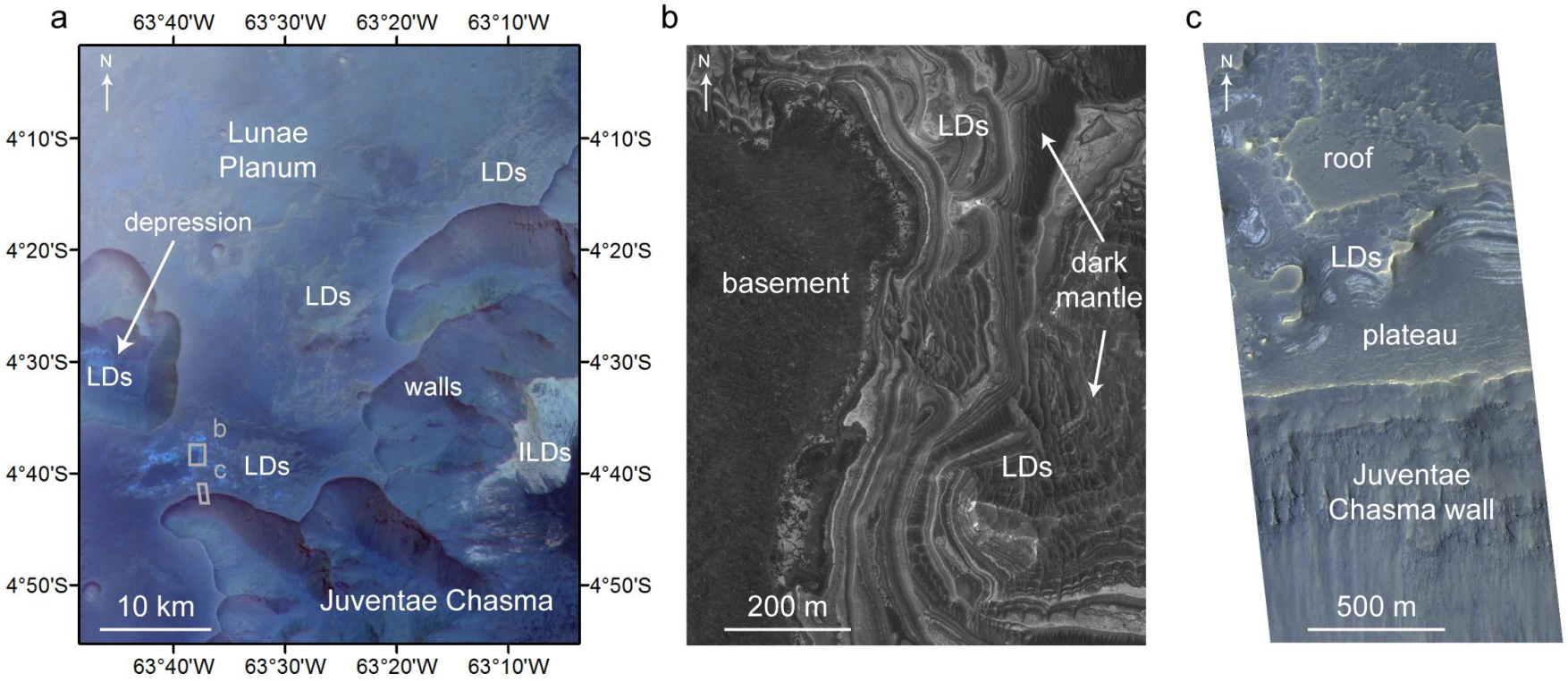
a
63°40'W
63°30'W
63°20'W
63°10'W
N
4°10'S
4°20'S
4°30'S
4°40'S
4°50'S
Lunae Planum
LDs
depression
LDs
LDs
walls
b
c
LDs
ILDs
10 km
Juventae Chasma
b
N
LDs
basement
dark mantle
LDs
200 m
c
N
roof
LDs
plateau
Juventae Chasma wall
500 m

Figure 2

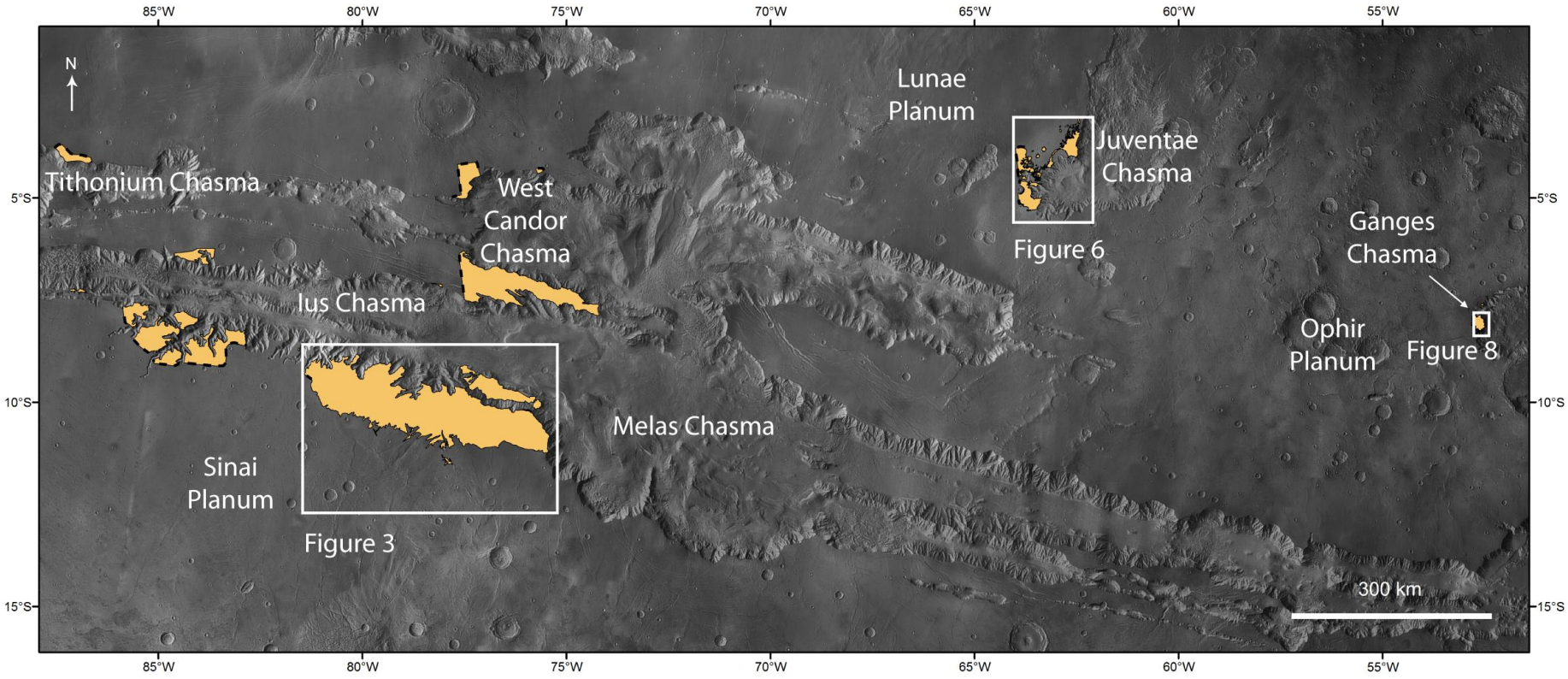
85°W
80°W
75°W
70°W
65°W
60°W
55°W
N
Lunae
Planum
Juventae
Chasma
Figure 6
Tithonium Chasma
West
Candor
Chasma
Ganges
Chasma
Ius Chasma
Ophir
Planum
Figure 8
5°S
10°S
15°S
Melas Chasma
Sinai
Planum
Figure 3
300 km

Figure 3

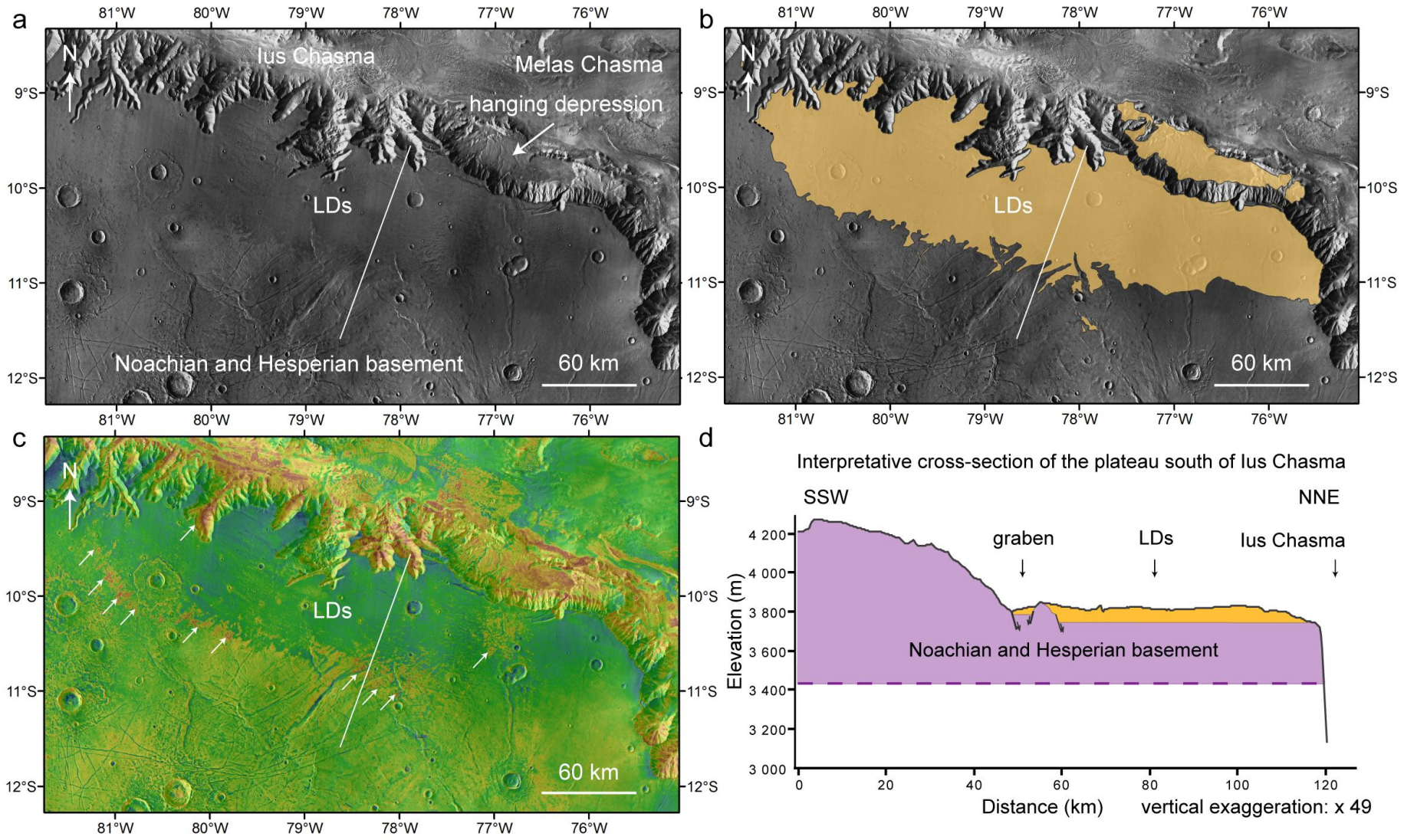
a
b
c
d
81°W
80°W
79°W
78°W
77°W
76°W
9°S
10°S
11°S
12°S
N
Ius Chasma
Melas Chasma
hanging depression
LDs
Noachian and Hesperian basement
60 km
Interpretative cross-section of the plateau south of Ius Chasma
SSW
NNE
graben
LDs
Ius Chasma
Noachian and Hesperian basement
Elevation (m)
4 200
4 000
3 800
3 600
3 400
3 200
3 000
0
20
40
60
80
100
120
Distance (km)
vertical exaggeration: x 49

Figure 4

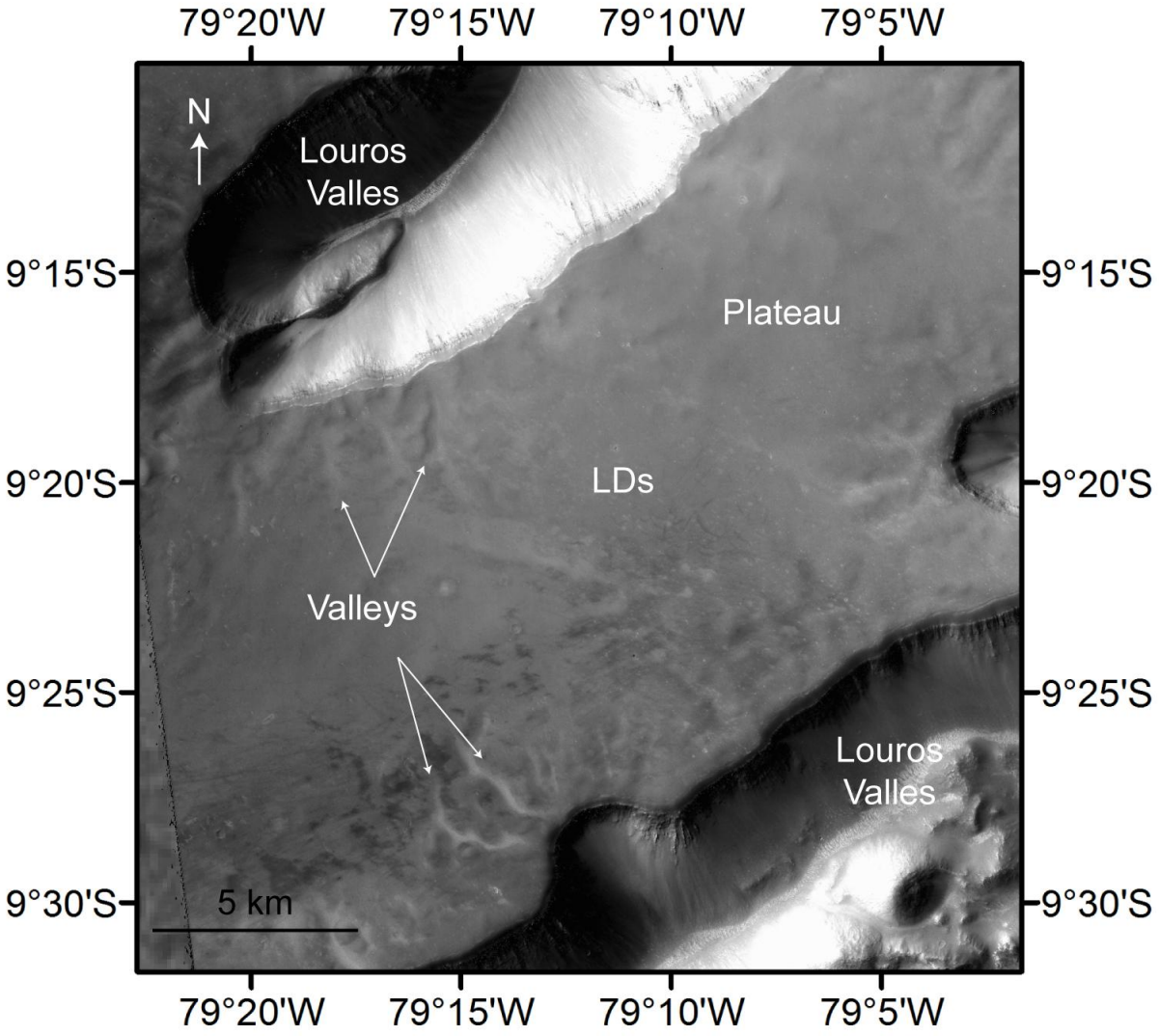
79°20'W
79°15'W
79°10'W
79°5'W
N
Louros
Valles
9°15'S
Plateau
9°20'S
LDs
Valleys
9°25'S
Louros
Valles
9°30'S
5 km

Figure 5

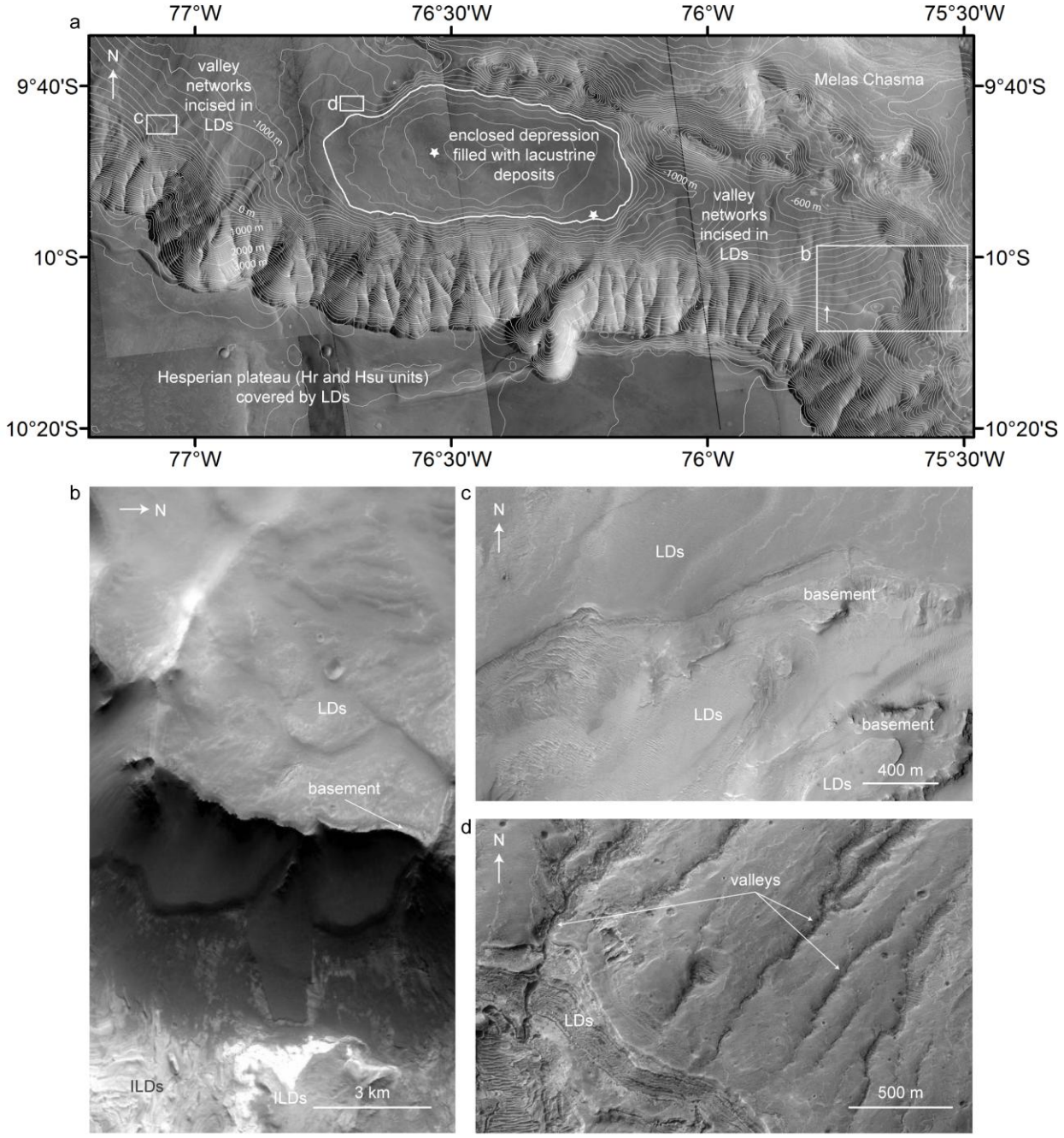
a
77°W
76°30'W
76°W
75°30'W
9°40'S
10°S
10°20'S
N
valley networks incised in LDs
c
d
enclosed depression filled with lacustrine deposits
Melas Chasma
valley networks incised in LDs
b
Hesperian plateau (Hr and Hsu units) covered by LDs
b
N
LDs
basement
lLDs
lLDs
3 km
c
N
LDs
basement
LDs
basement
LDs
400 m
d
N
valleys
LDs
500 m

Figure 6

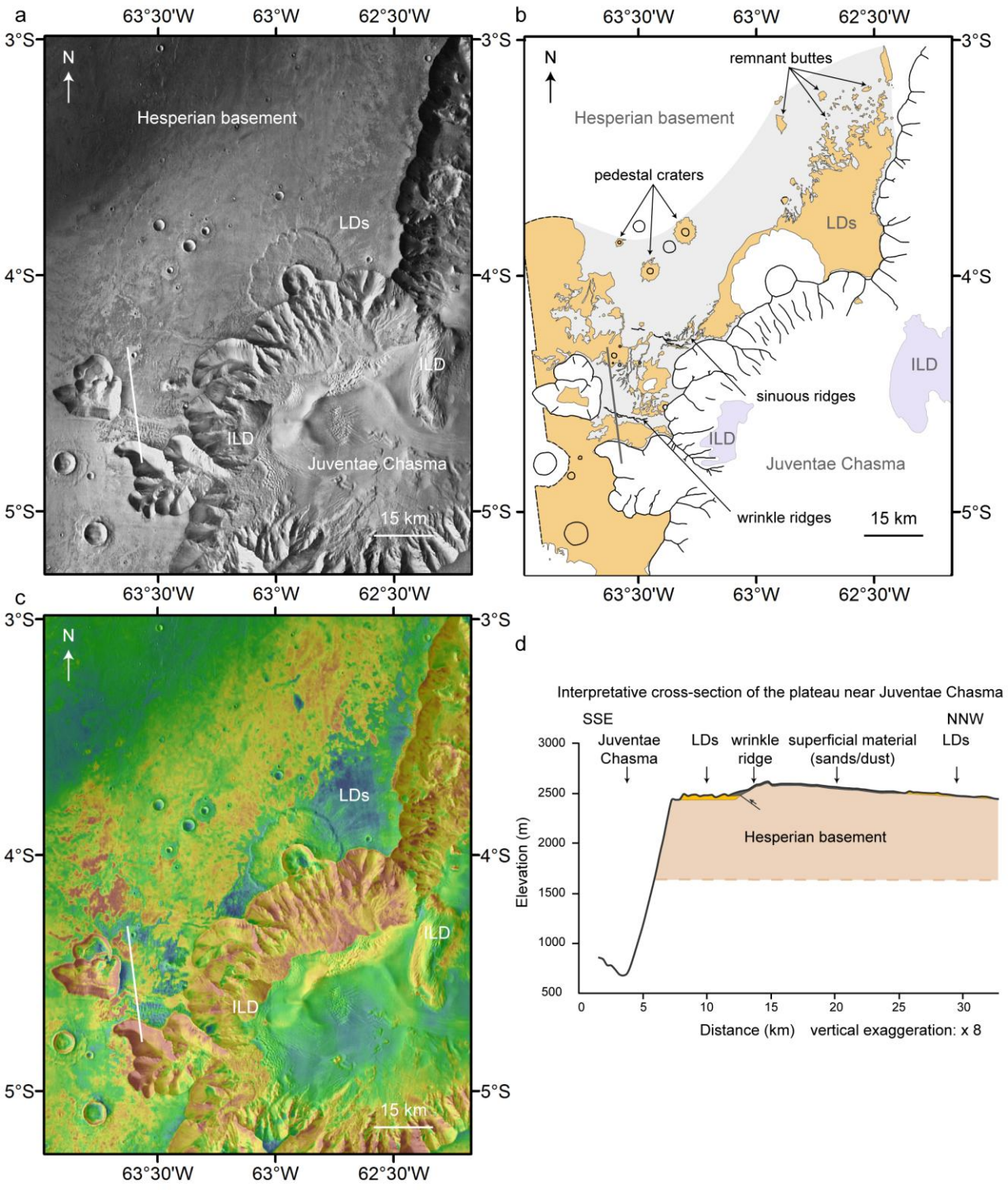
a
b
c
d
63°30'W
63°W
62°30'W
3°S
4°S
5°S
N
Hesperian basement
LDs
ILD
Juventae Chasma
15 km
remnant buttes
pedestal craters
sinuous ridges
wrinkle ridges
Interpretative cross-section of the plateau near Juventae Chasma
SSE
NNW
Juventae Chasma
LDs
wrinkle ridge
superficial material (sands/dust)
Elevation (m)
3000
2500
2000
1500
1000
500
0
5
10
15
20
25
30
Distance (km)
vertical exaggeration: x 8

Figure 7

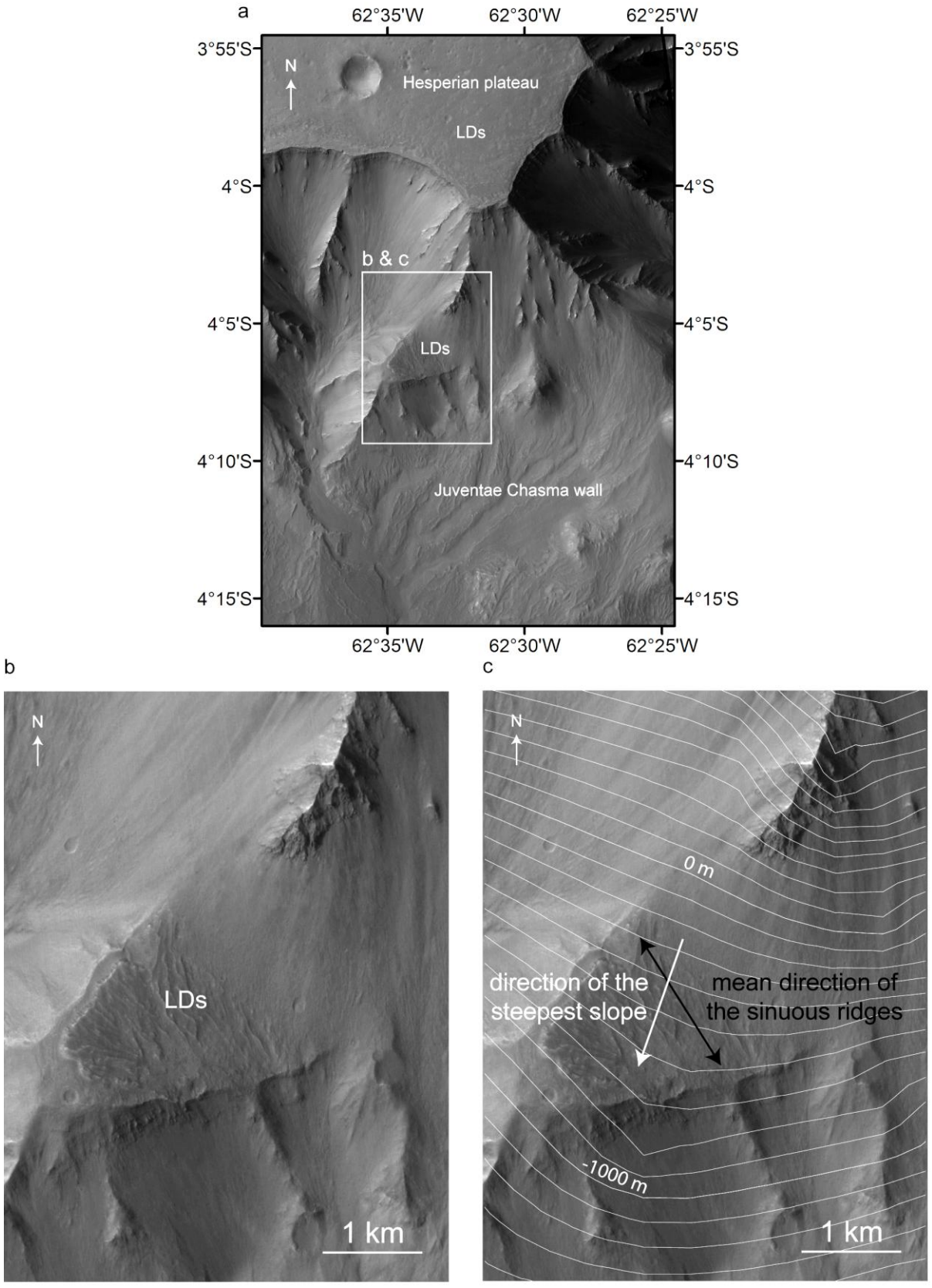
a
62°35'W
62°30'W
62°25'W
3°55'S
4°S
4°5'S
4°10'S
4°15'S
N
Hesperian plateau
LDs
b & c
LDs
Juventae Chasma wall
b
N
LDs
1 km
c
N
0 m
-1000 m
direction of the steepest slope
mean direction of the sinuous ridges
1 km

Figure 8

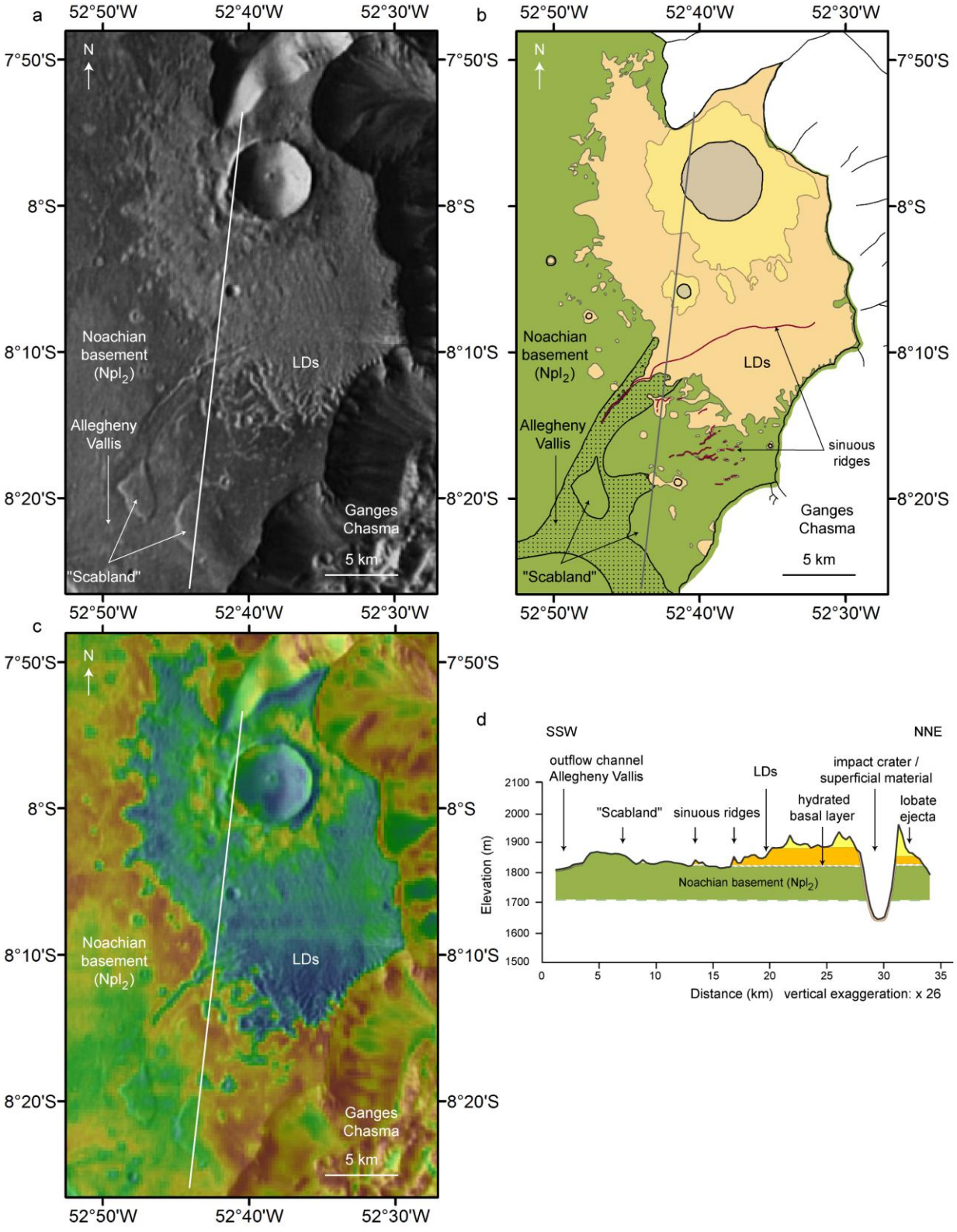
a
b
c
d
52°50'W
52°40'W
52°30'W
7°50'S
8°S
8°10'S
8°20'S
N
Noachian basement (Npl2)
LDs
Allegheny Vallis
"Scabland"
Ganges Chasma
5 km
sinuous ridges
SSW
NNE
outflow channel Allegheny Vallis
impact crater / superficial material
hydrated basal layer
lobate ejecta
Elevation (m)
2100
2000
1900
1800
1700
1600
1500
0
5
10
15
20
25
30
35
Distance (km)
vertical exaggeration: x 26

Figure 9

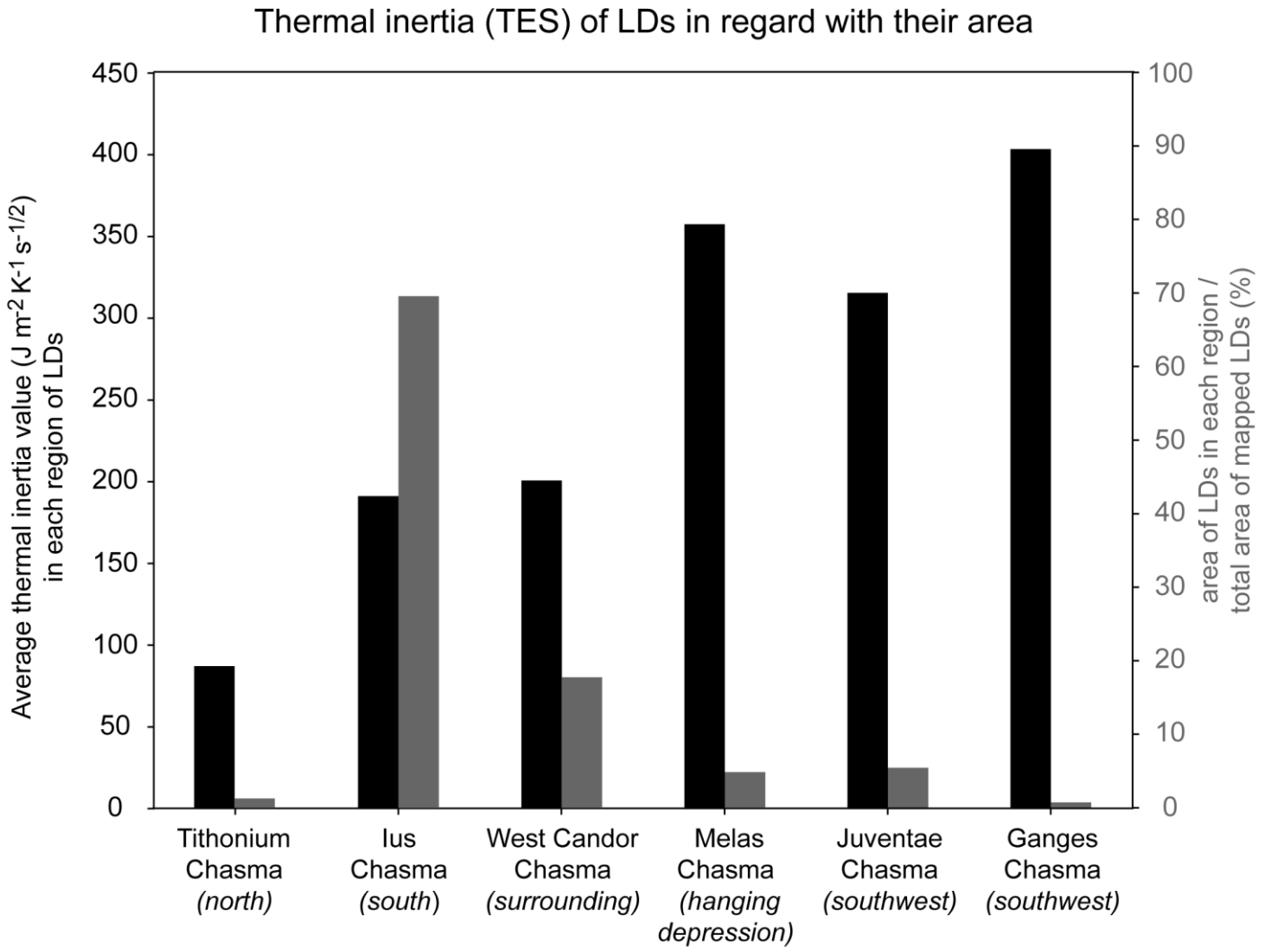
Thermal inertia (TES) of LDs in regard with their area
Average thermal inertia value (J m-2 K-1 s-1/2) in each region of LDs
area of LDs in each region / total area of mapped LDs (%)
450
400
350
300
250
200
150
100
50
0
100
90
80
70
60
50
40
30
20
10
0
Tithonium Chasma (north)
Ius Chasma (south)
West Candor Chasma (surrounding)
Melas Chasma (hanging depression)
Juventae Chasma (southwest)
Ganges Chasma (southwest)

Figure 10

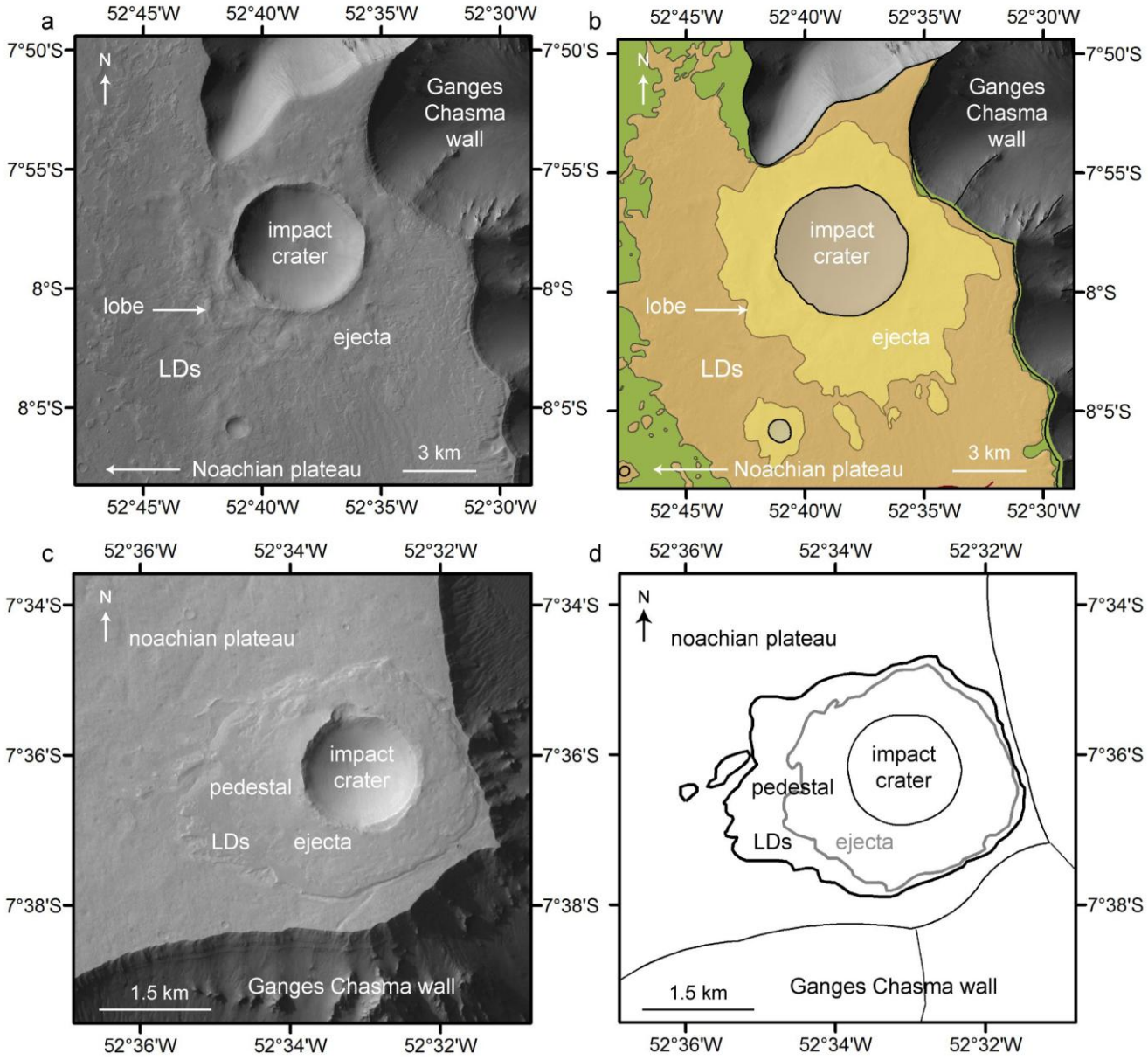
a
b
c
d
52°45'W
52°40'W
52°35'W
52°30'W
7°50'S
7°55'S
8°S
8°5'S
N
Ganges Chasma wall
impact crater
lobe
ejecta
LDs
Noachian plateau
3 km
52°36'W
52°34'W
52°32'W
7°34'S
7°36'S
7°38'S
noachian plateau
pedestal
1.5 km

Figure 11

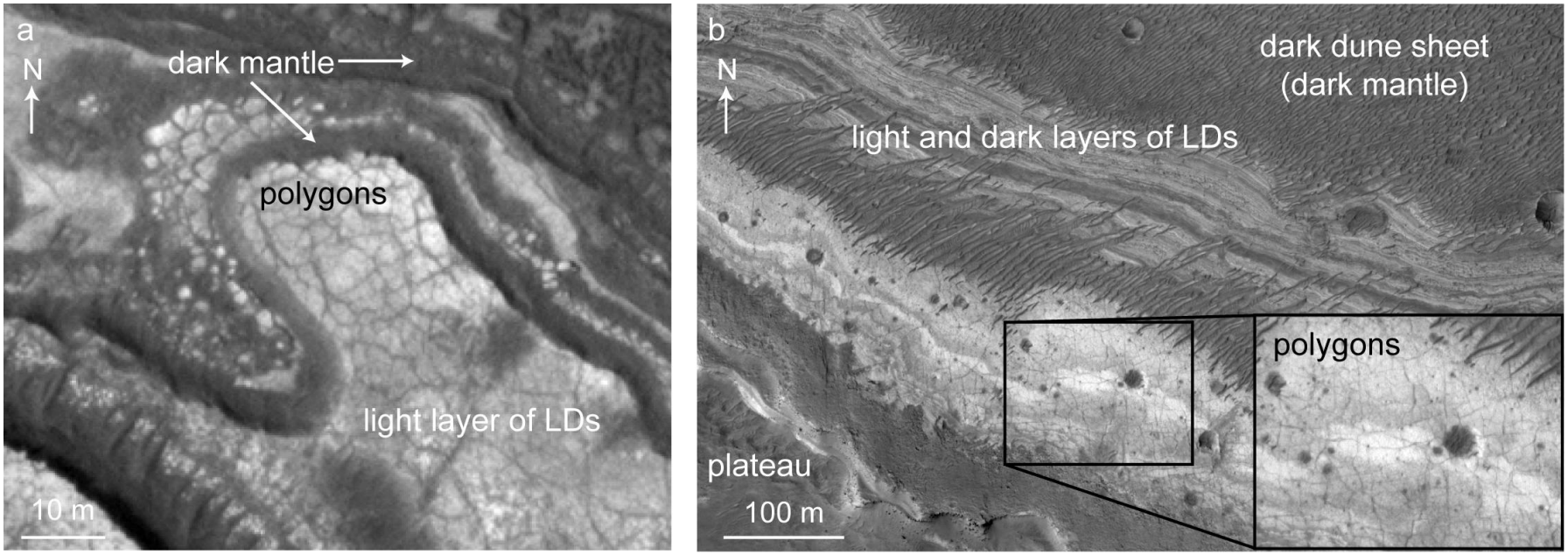
a
N
dark mantle
polygons
light layer of LDs
10 m
b
N
dark dune sheet
(dark mantle)
light and dark layers of LDs
polygons
plateau
100 m

Figure 12

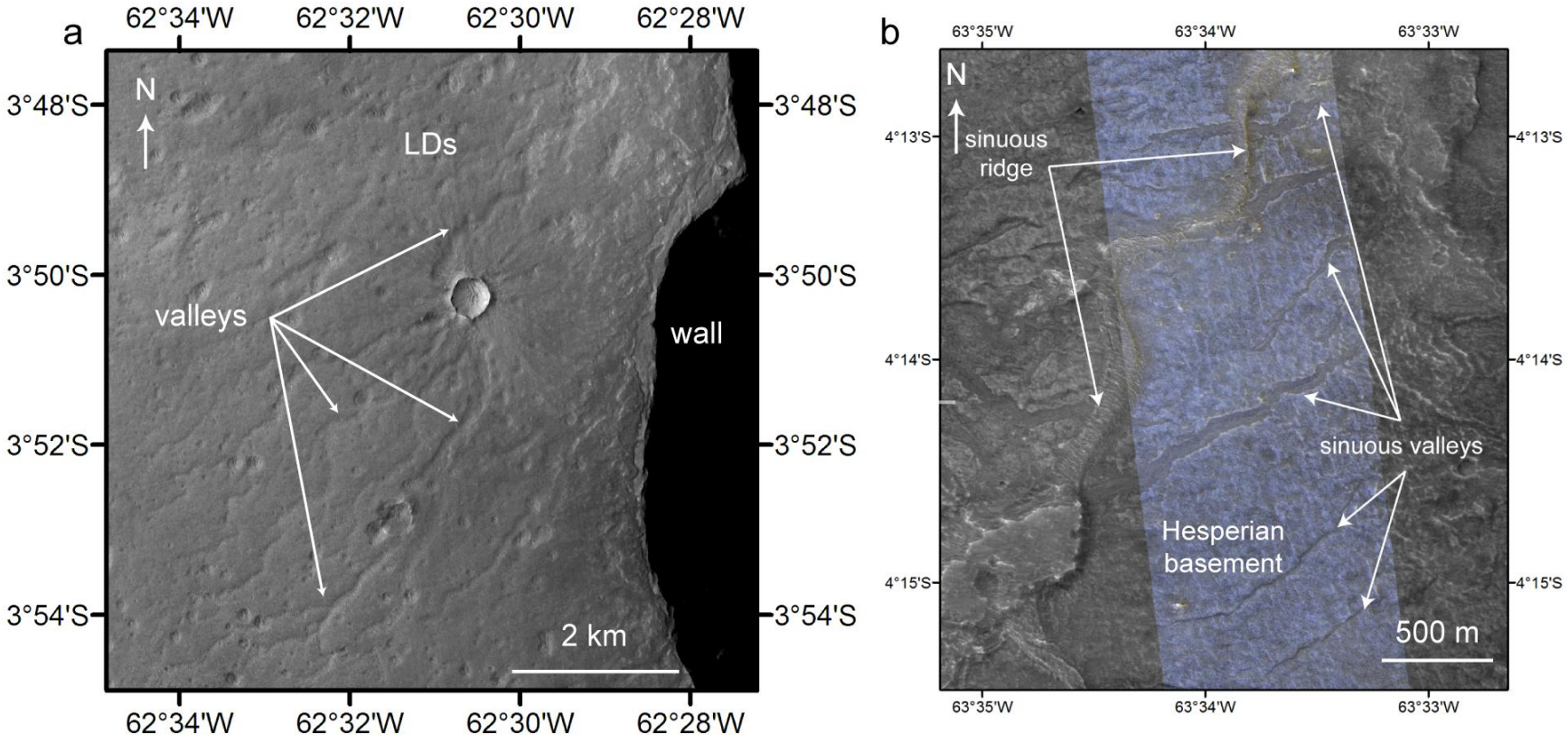
a
62°34'W
62°32'W
62°30'W
62°28'W
N
3°48'S
3°50'S
3°52'S
3°54'S
LDs
valleys
wall
2 km
b
63°35'W
63°34'W
63°33'W
N
4°13'S
4°14'S
4°15'S
sinuous ridge
sinuous valleys
Hesperian basement
500 m

Figure 13

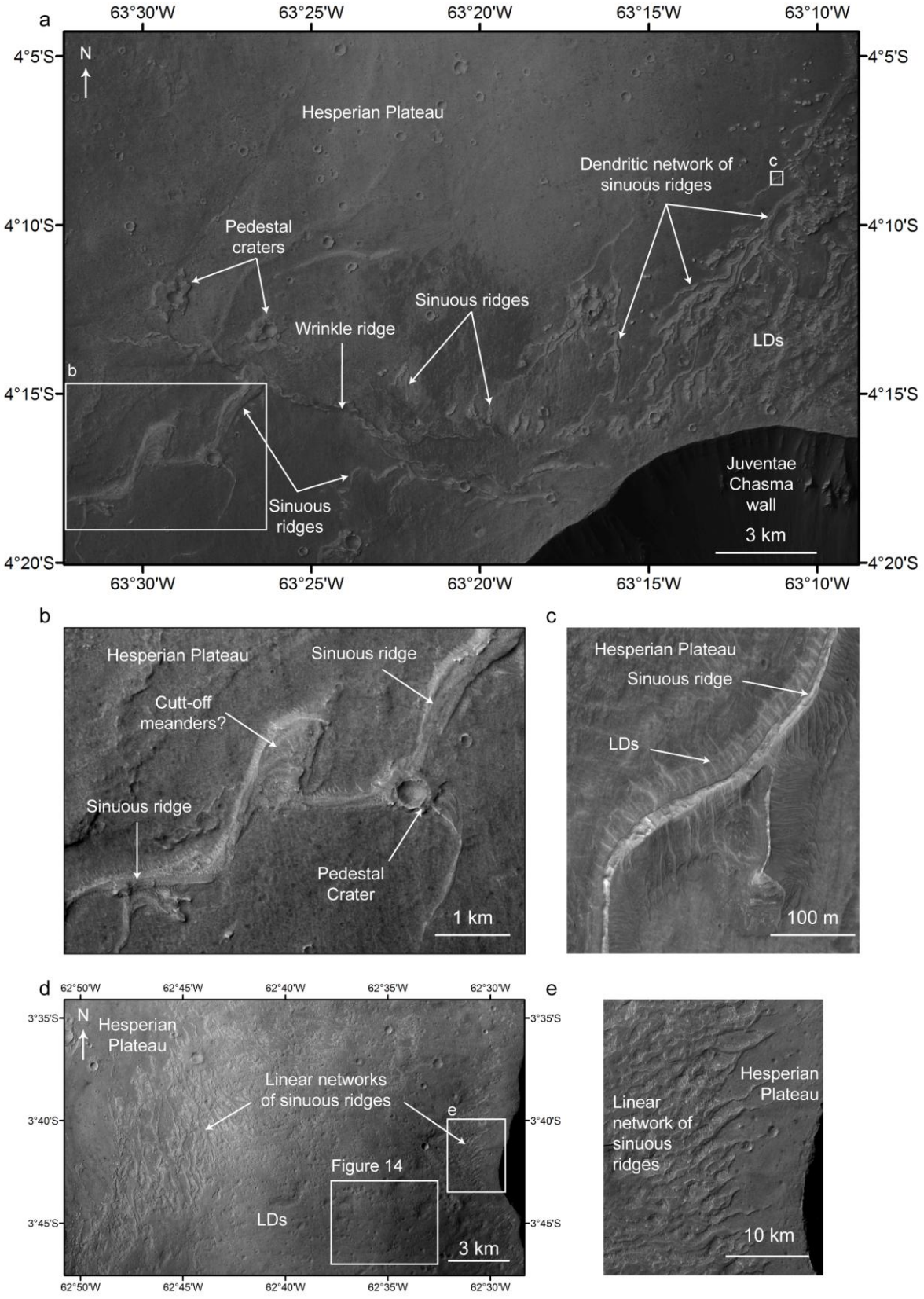
a
63°30'W
63°25'W
63°20'W
63°15'W
63°10'W
4°5'S
4°10'S
4°15'S
4°20'S
N
Hesperian Plateau
Dendritic network of sinuous ridges
c
Pedestal craters
Sinuous ridges
Wrinkle ridge
LDs
b
Juventae Chasma wall
Sinuous ridges
3 km
b
Hesperian Plateau
Sinuous ridge
Cutt-off meanders?
Sinuous ridge
Pedestal Crater
1 km
c
Hesperian Plateau
Sinuous ridge
LDs
100 m
d
62°50'W
62°45'W
62°40'W
62°35'W
62°30'W
3°35'S
3°40'S
3°45'S
N
Hesperian Plateau
Linear networks of sinuous ridges
e
Figure 14
LDs
3 km
e
Hesperian Plateau
Linear network of sinuous ridges
10 km

Figure 14

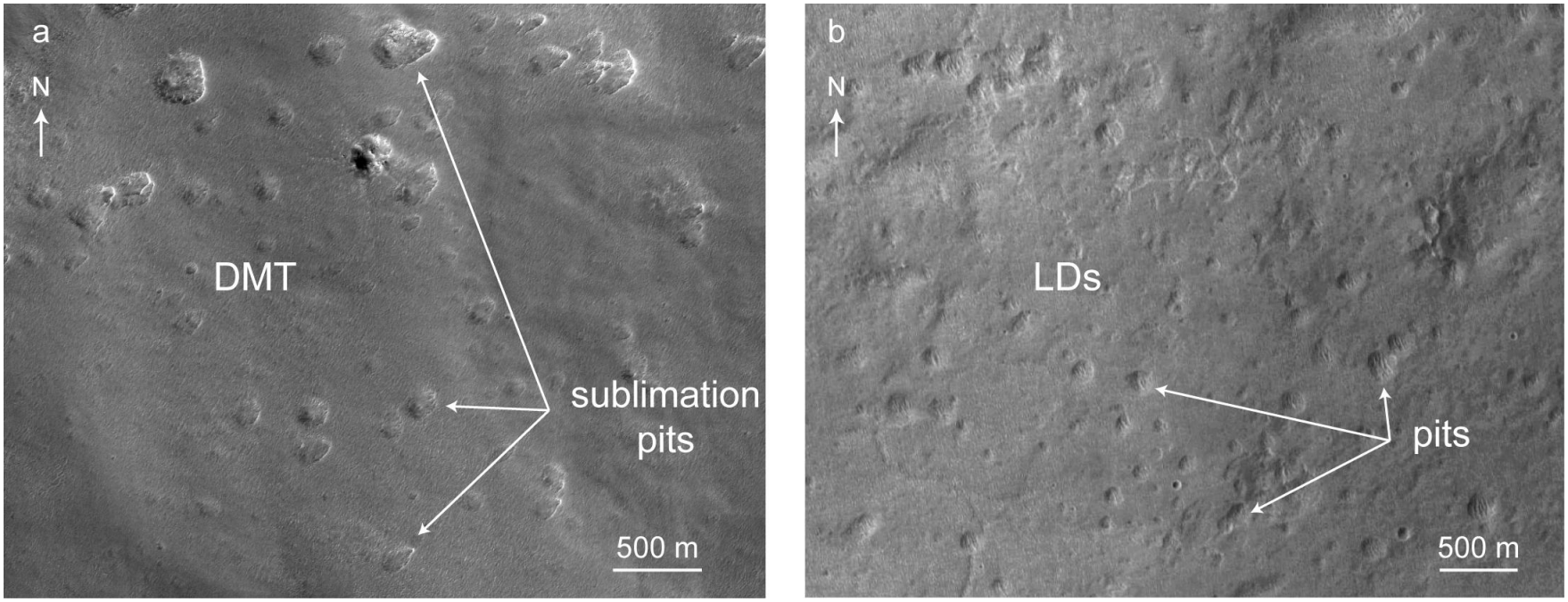

Figure 15

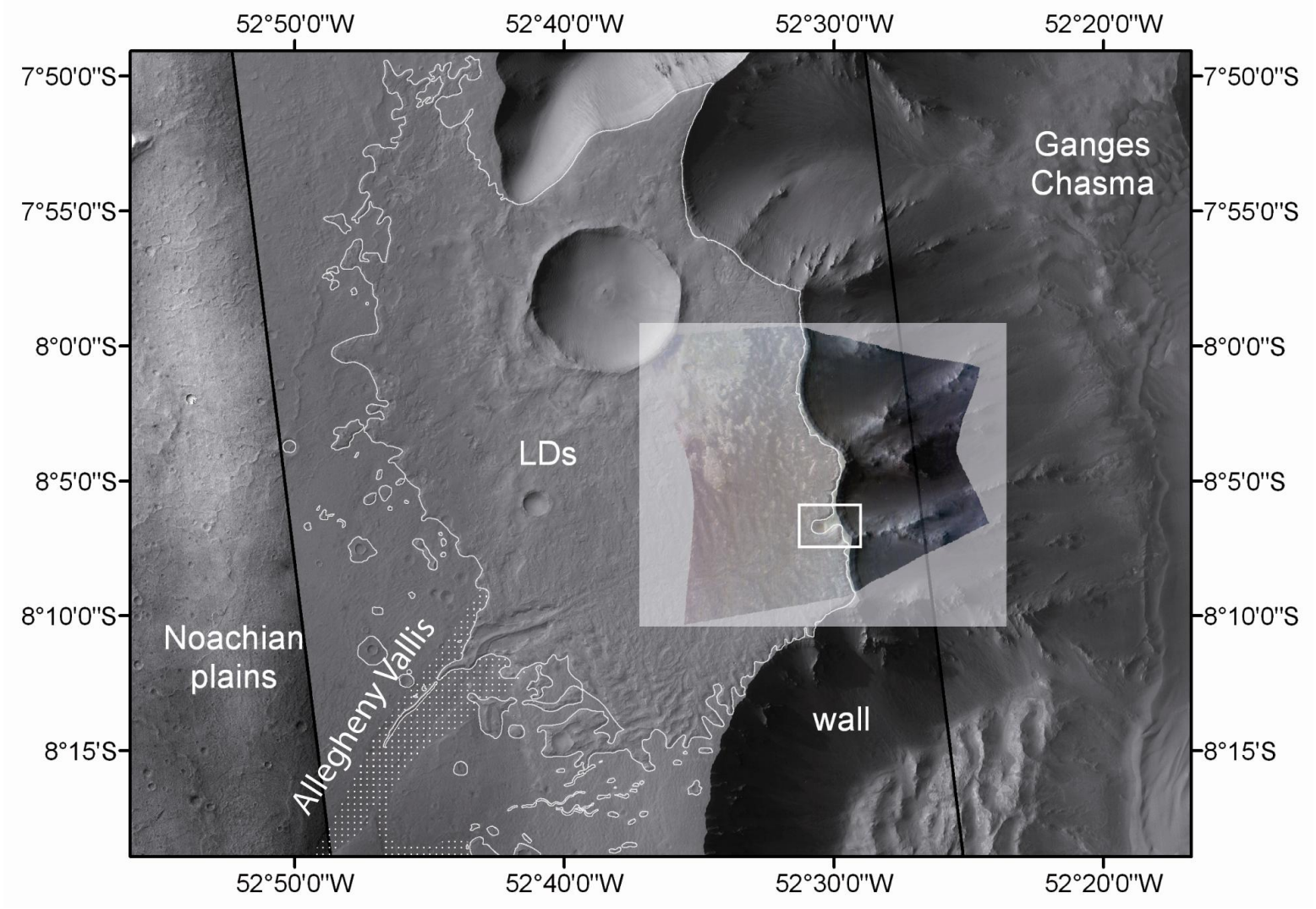
52°50'0"W
52°40'0"W
52°30'0"W
52°20'0"W
7°50'0"S
7°55'0"S
8°0'0"S
8°5'0"S
8°10'0"S
8°15'S
Ganges Chasma
LDs
Noachian plains
Allegheny Vallis
wall

Figure 16

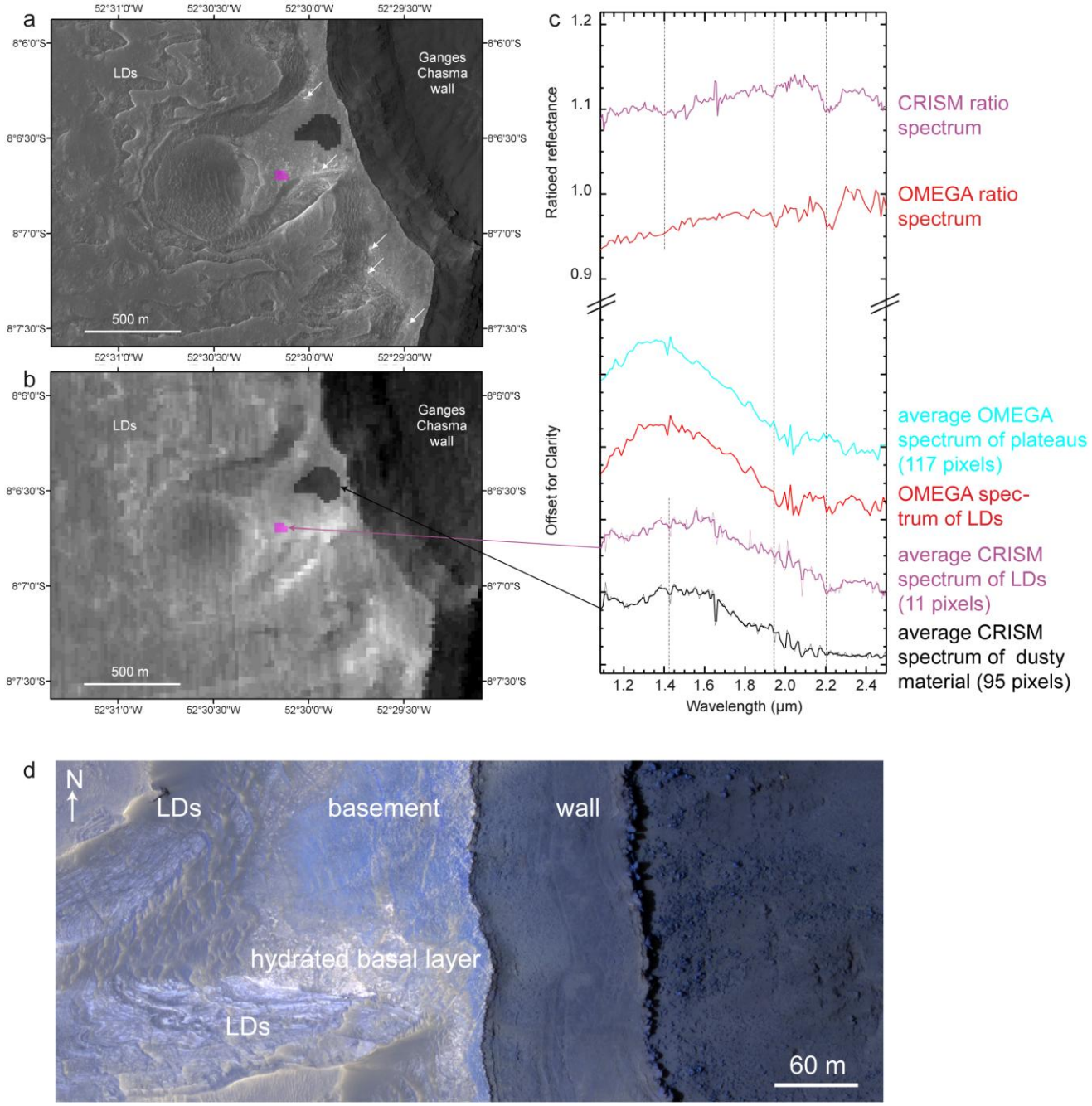
a
b
c
d
LDs
Ganges Chasma wall
500 m
52°31'0"W
52°30'30"W
52°30'0"W
52°29'30"W
8°6'0"S
8°6'30"S
8°7'0"S
8°7'30"S
Ratioed reflectance
Offset for Clarity
Wavelength (μm)
CRISM ratio spectrum
OMEGA ratio spectrum
average OMEGA spectrum of plateaus (117 pixels)
OMEGA spectrum of LDs
average CRISM spectrum of LDs (11 pixels)
average CRISM spectrum of dusty material (95 pixels)
N
basement
wall
hydrated basal layer
60 m

Figure 17

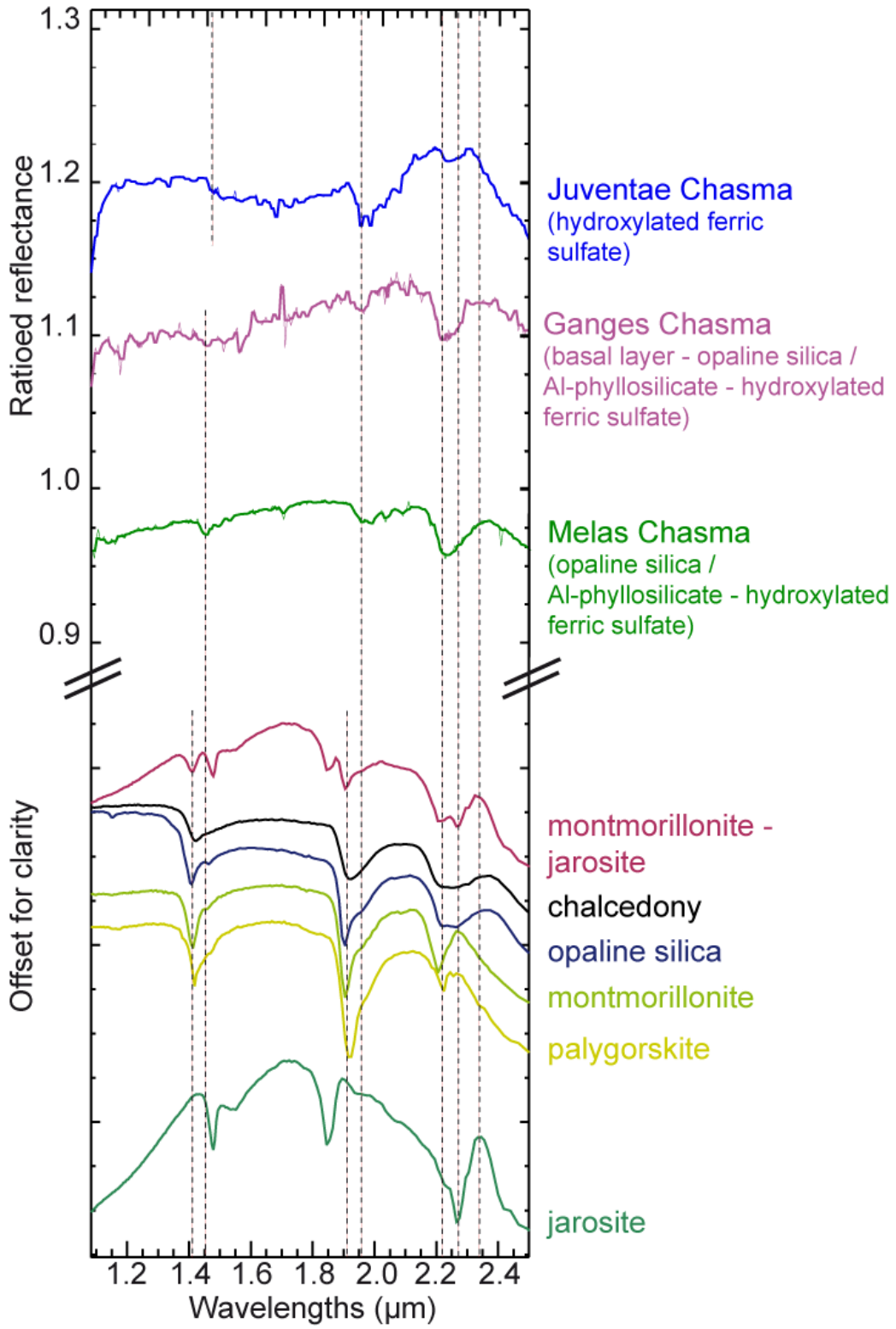
1.3
1.2
1.1
1.0
0.9
Ratioed reflectance
Juventae Chasma
(hydroxylated ferric sulfate)
Ganges Chasma
(basal layer - opaline silica / Al-phyllosilicate - hydroxylated ferric sulfate)
Melas Chasma
(opaline silica / Al-phyllosilicate - hydroxylated ferric sulfate)
Offset for clarity
montmorillonite - jarosite
chalcedony
opaline silica
montmorillonite
palygorskite
jarosite
1.2 1.4 1.6 1.8 2.0 2.2 2.4
Wavelengths (μm)

Figure 18

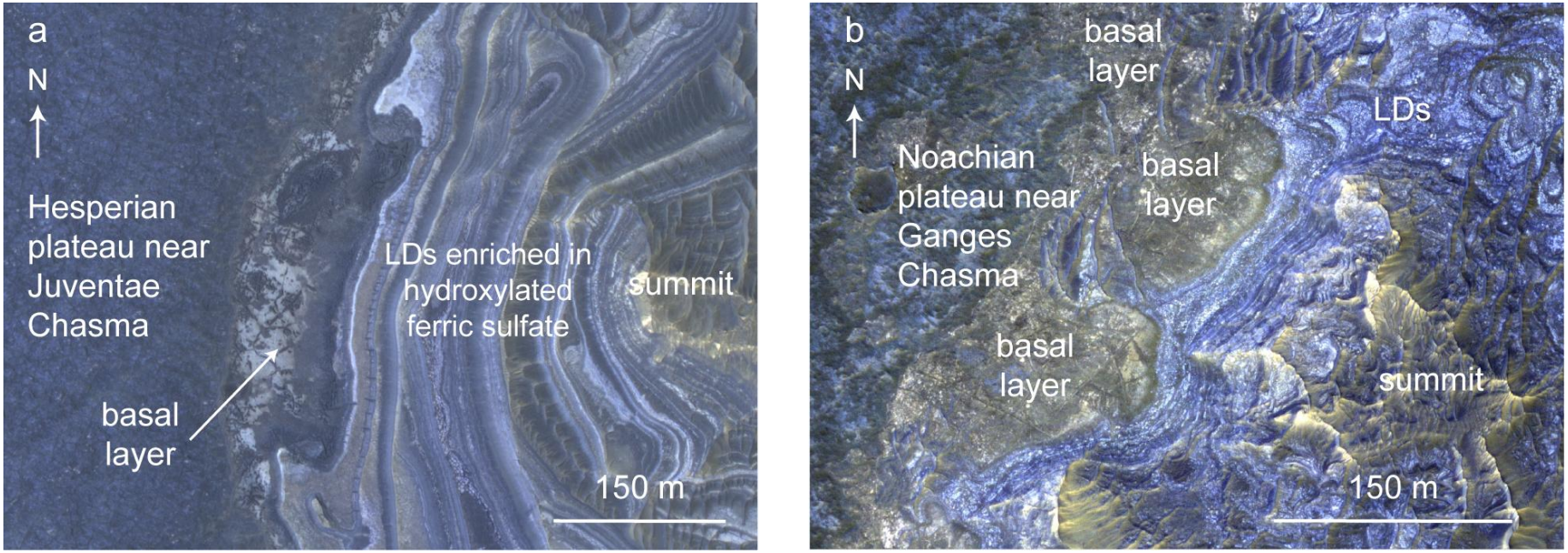
a
N
Hesperian plateau near Juventae Chasma
basal layer
LDs enriched in hydroxylated ferric sulfate
summit
150 m
b
N
basal layer
LDs
Noachian plateau near Ganges Chasma
basal layer
basal layer
summit
150 m

Figure 19

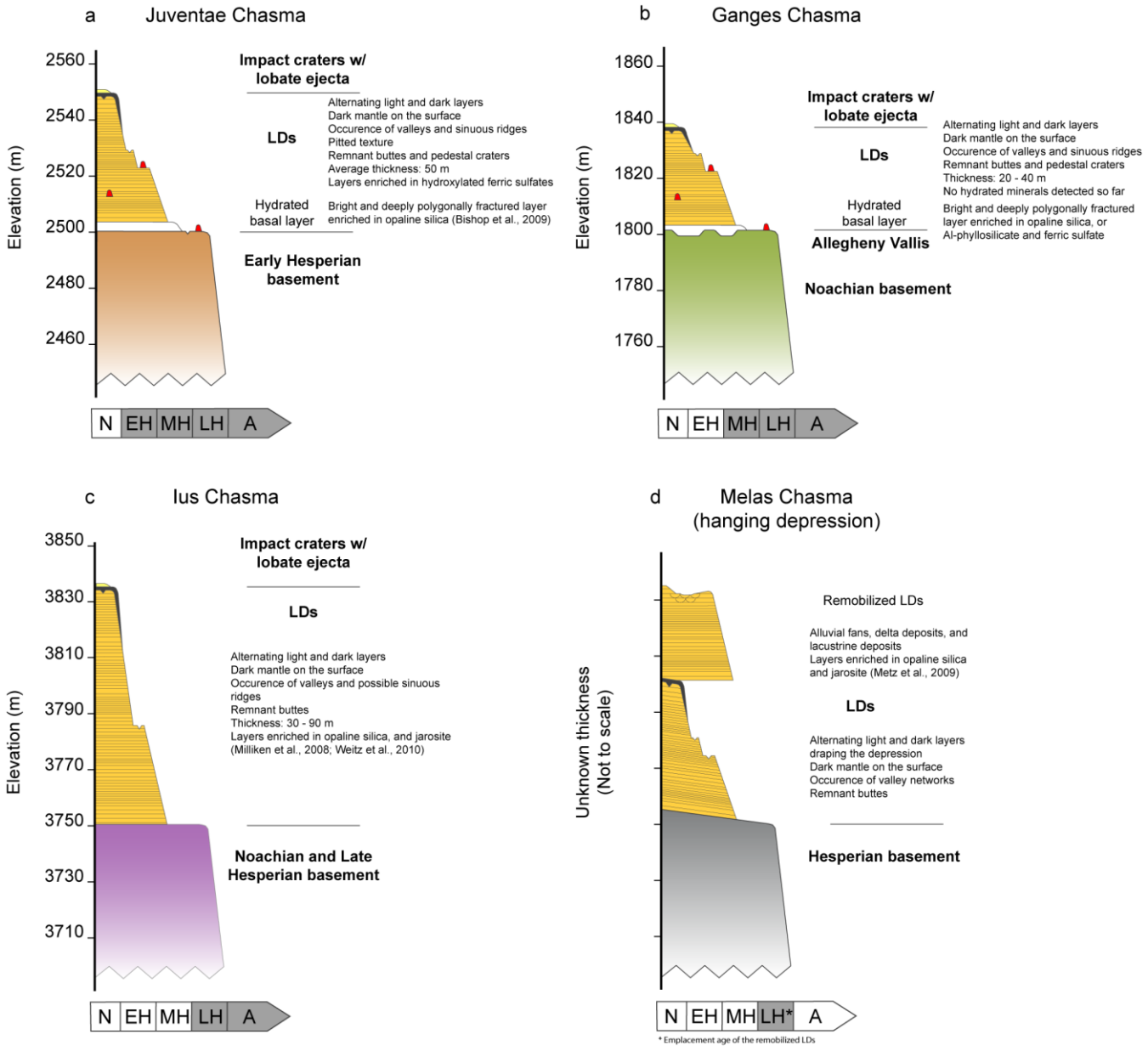
a
Juventae Chasma
Elevation (m)
2560
2540
2520
2500
2480
2460
Impact craters w/ lobate ejecta
LDs
Alternating light and dark layers
Dark mantle on the surface
Occurence of valleys and sinuous ridges
Pitted texture
Remnant buttes and pedestal craters
Average thickness: 50 m
Layers enriched in hydroxylated ferric sulfates
Hydrated basal layer
Bright and deeply polygonally fractured layer enriched in opaline silica (Bishop et al., 2009)
Early Hesperian basement
N EH MH LH A
b
Ganges Chasma
Elevation (m)
1860
1840
1820
1800
1780
1760
Impact craters w/ lobate ejecta
LDs
Alternating light and dark layers
Dark mantle on the surface
Occurence of valleys and sinuous ridges
Remnant buttes and pedestal craters
Thickness: 20 - 40 m
No hydrated minerals detected so far
Hydrated basal layer
Allegheny Vallis
Bright and deeply polygonally fractured layer enriched in opaline silica, or Al-phyllosilicate and ferric sulfate
Noachian basement
N EH MH LH A
c
Ius Chasma
Elevation (m)
3850
3830
3810
3790
3770
3750
3730
3710
Impact craters w/ lobate ejecta
LDs
Alternating light and dark layers
Dark mantle on the surface
Occurence of valleys and possible sinuous ridges
Remnant buttes
Thickness: 30 - 90 m
Layers enriched in opaline silica, and jarosite (Milliken et al., 2008; Weitz et al., 2010)
Noachian and Late Hesperian basement
N EH MH LH A
d
Melas Chasma
(hanging depression)
Unknown thickness
(Not to scale)
Remobilized LDs
Alluvial fans, delta deposits, and lacustrine deposits
Layers enriched in opaline silica and jarosite (Metz et al., 2009)
LDs
Alternating light and dark layers draping the depression
Dark mantle on the surface
Occurence of valley networks
Remnant buttes
Hesperian basement
N EH MH LH* A
* Emplacement age of the remobilized LDs